Virus-Induced Alterations in Primary Metabolism Modulate Susceptibility to *Tobacco rattle virus* in Arabidopsis[1][C][W]

Lourdes Fernández-Calvino[2], Sonia Osorio[3], M. Luisa Hernández, Ignacio B. Hamada, Francisco J. del Toro, Livia Donaire, Agnés Yu[4], Regla Bustos, Alisdair R. Fernie, José M. Martínez-Rivas, and César Llave*

Centro de Investigaciones Biológicas, Consejo Superior de Investigaciones Científicas, 28040 Madrid, Spain (L.F.-C., I.B.H., F.J.d.T., L.D., C.L.); Max Planck Institute for Molecular Plant Physiology, 14476 Postdam-Golm, Germany (S.O., A.R.F.); Instituto de la Grasa, Consejo Superior de Investigaciones Científicas, 41012 Seville, Spain (M.L.H., J.M.M.-R.); Unité de Recherche en Génomique Végétale, 91057 Evry cedex, France (A.Y.); and Centro de Biotecnología y Genómica de Plantas, Campus Montegancedo, Pozuelo de Alarcón, 28223 Madrid, Spain (R.B.)

During compatible virus infections, plants respond by reprogramming gene expression and metabolite content. While gene expression studies are profuse, our knowledge of the metabolic changes that occur in the presence of the virus is limited. Here, we combine gene expression and metabolite profiling in Arabidopsis (*Arabidopsis thaliana*) infected with *Tobacco rattle virus* (TRV) in order to investigate the influence of primary metabolism on virus infection. Our results revealed that primary metabolism is reconfigured in many ways during TRV infection, as reflected by significant changes in the levels of sugars and amino acids. Multivariate data analysis revealed that these alterations were particularly conspicuous at the time points of maximal accumulation of TRV, although infection time was the dominant source of variance during the process. Furthermore, TRV caused changes in lipid and fatty acid composition in infected leaves. We found that several Arabidopsis mutants deficient in branched-chain amino acid catabolism or fatty acid metabolism possessed altered susceptibility to TRV. Finally, we showed that increments in the putrescine content in TRV-infected plants correlated with enhanced tolerance to freezing stress in TRV-infected plants and that impairment of putrescine biosynthesis promoted virus multiplication. Our results thus provide an interesting overview for a better understanding of the relationship between primary metabolism and virus infection.

A compatible virus infection in plants is a multifaceted and controlled process whereby the virus appropriates cellular functions in order to replicate and move throughout the plant. In this complex interaction, plants accommodate their metabolism to restrict virus infection and to counteract potential adverse effects caused by the virus (Whitham et al., 2006). By using gene expression profiling tools that monitor the expression of host mRNA transcripts on a genome-wide scale and bioinformatics approaches for functional categorization of virus-responsive genes, we can deduce cellular processes and pathways linked to the infection process (Wise et al., 2007). In general, both the type and number of genes that are either up- or down-regulated during infections differ substantially in distinct experimental systems and sampling procedures. Nevertheless, comparative analyses have revealed extensive convergence in the biological functions that are broadly perturbed upon viral attack (Whitham et al., 2003; Espinoza et al., 2007). However, despite of the proliferation in transcriptomic data, elucidation of the pathways that are instrumental for the infection to take place is often complicated.

In general, pathogen-triggered responses are associated with increasing demands for energy, reducing equivalents, and carbon skeletons that are provided by primary metabolic pathways (Berger et al., 2007; Bolton, 2009). While metabolic changes associated with infection by fungi and bacteria have been widely documented (Bolton, 2009), little is known about the effect of plant viruses on host primary metabolites and the influence

[1] This work was supported by the Spanish Ministry of Science and Innovation (grant nos. BIO2006–13107 and BIO2009–12004, graduate fellowships to F.J.d.T. and I.B.H., and Ramón and Cajal contract to S.O.), by the Andalusian Government, Spain (grant no. P09–AGR–4516), and by the Consejo Superior de Investigaciones Científicas (Junta de Ampliación de Estudios-Doctores contracts to L.F.-C. and M.L.H.).

[2] Present address: Centro de Biotecnología y Genómica de Plantas, Campus Montegancedo, Pozuelo de Alarcón, 28223 Madrid, Spain.

[3] Present address: Instituto de Hortofruticultura Subtropical y Mediterránea, Universidad de Málaga-Consejo Superior de Investigaciones Científicas, Departamento de Biología Molecular y Bioquímica, Facultad de Ciencias, 29071 Malaga, Spain.

[4] Present address: Ecole Normale Supérieure/Centre National de la Recherche Scientifique-Unité Mixte de Recherche 8197, Institut de Biologie de l'Ecole Normale Superieure, Biologie Moléculaire des Organismes Photosynthétiques, 46 rue d'Ulm, 75230 Paris cedex 05, France.

* Address correspondence to cesarllave@cib.csic.es.

The author responsible for distribution of materials integral to the findings presented in this article in accordance with the policy described in the Instructions for Authors (www.plantphysiol.org) is: César Llave (cesarllave@cib.csic.es).

[C] Some figures in this article are displayed in color online but in black and white in the print edition.

[W] The online version of this article contains Web-only data.

www.plantphysiol.org/cgi/doi/10.1104/pp.114.250340

of these changes on the onset of infection and symptom expression. Traditionally, most studies were devoted to elucidate how plant viruses interfere with carbohydrate metabolism (Herbers et al., 1996; Almon et al., 1997; Balachandran et al., 1997; Herbers et al., 2000; Shalitin and Wolf, 2000). More recently, the advent of metabolomics has allowed the characterization of plant metabolite profiles thorough the detection of a large number of metabolites in target organs (Lisec et al., 2006; Kim et al., 2010). As a result, it is now possible to unmask chemical compounds implicated in compatible or defense responses against viruses and evaluate their contribution to the infectious process (Xu et al., 2008; Bazzini et al., 2011; López-Gresa et al., 2012).

Liquid chromatography and gas chromatography-mass spectrometry (GC-MS) have been used to determine the relative levels of metabolites across viral infections. For instance, a significant increment in the levels of multiple metabolites was observed at an early time point after infection with *Tobacco mosaic virus*, including a group of sugars and organic acids associated with the tricarboxylic acid cycle (Bazzini et al., 2011). At later stages of infection, alterations include both increases and decreases in metabolites that correlate with virus accumulation levels (Bazzini et al., 2011). GC-MS-based metabolomics was also used to report the increment of several osmoprotectant and antioxidant compounds in virus-infected plants, which in turn made plants more tolerant to abiotic stresses (Xu et al., 2008). NMR has been used to study alterations on the metabolome triggered by *Tobacco mosaic virus* in tomato (*Solanum lycopersicum*; López-Gresa et al., 2012) and tobacco (*Nicotiana tabacum*; Choi et al., 2006) leaves. These studies identified a set of metabolites induced during the plant defense response as well as metabolites whose accumulation depends on factors such as developmental stage, position on the plant, and time of harvesting.

Here, we conducted transcriptional and metabolite profiling of Arabidopsis (*Arabidopsis thaliana*) infected with *Tobacco rattle virus* (TRV) in order to study the reciprocal influence between primary metabolism and virus infection.

RESULTS

Expression Profiling and Functional Categorization of TRV-Responsive Genes

We analyzed mRNA profiles in Arabidopsis leaves infected systemically with TRV. Given that virus-triggered responses generally occur in proportion to the amount of virus (Yang et al., 2007), relative viral accumulation was measured using quantitative reverse transcription (qRT)-PCR at multiple time points after inoculation. TRV RNA1 accumulated to very low levels in systemically infected leaves at 3 and 5 d post inoculation (dpi). It reached its peak expression at 8 dpi and then decreased sharply to lower levels that remain constant with slight fluctuations from 12 to 22 dpi (Fig. 1A). Based on this observation, we chose to document global transcriptomic changes at 8 dpi using noninoculated rosette leaves collected from mock-inoculated plants and TRV-infected plants. Using the Complete Arabidopsis Transcriptome Microarray (CATMA) and following statistical analysis of the data with $P < 0.01$, the transcript levels of 1,189

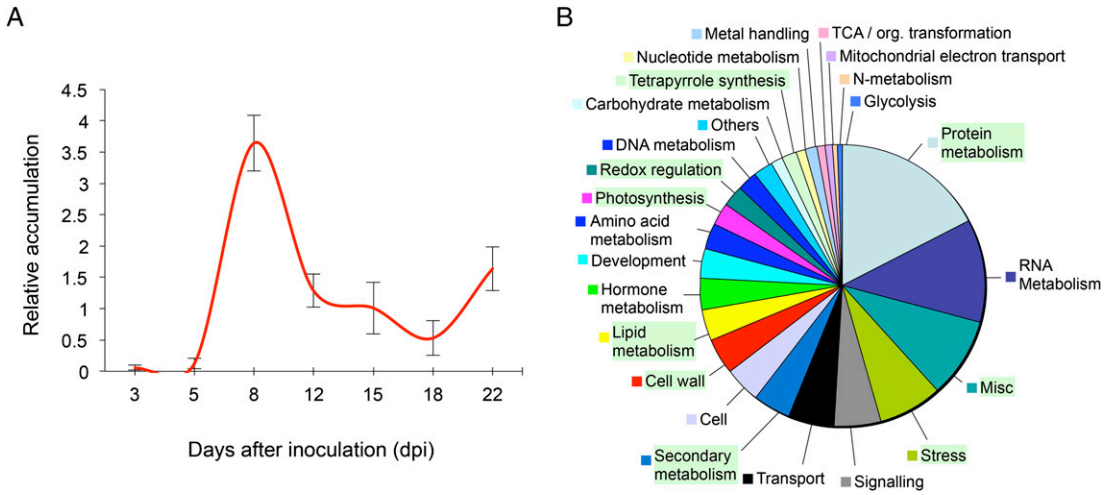

Figure 1. TRV accumulation and TRV-induced responses in the Arabidopsis transcriptome. A, Relative levels of TRV genomic RNA were measured in Arabidopsis leaves at time intervals after inoculation by qRT-PCR and expressed in arbitrary units after normalization to the *TUB5* internal control. B, Genes showing differential expression in response to TRV infection were sorted into known plant metabolic pathways or processes according to MapMan. Categories that were statistically overrepresented or underrepresented in each set of differentially expressed genes are highlighted (Fisher's exact test, $P < 0.001$). TCA, Tricarboxylic acid. [See online article for color version of this figure.]

genes (620 induced and 569 repressed) were significantly perturbed, with a more than 1.5-fold increase or decrease in signal intensity in TRV-infected samples compared with mock-inoculated controls (Supplemental Tables S1 and S2).

To determine which biological processes were affected by TRV infection in Arabidopsis, we used the MapMan metabolic pathway annotator, which classifies each altered gene according to its likely function (Thimm et al., 2004). The distribution of genes with known annotations among the MapMan functional categories indicated that TRV infection significantly modulates the expression of genes from several broad functional categories (Fig. 1B). A high percentage of repressed genes, not expected by chance, were assigned to the photosynthesis category (Fisher's exact test, P = 5.8E-11), including transcripts involved in light harvesting, photorespiration, and the Calvin cycle (Fig. 2A). In addition, genes related to tetrapyrrole metabolism and chlorophyll biosynthesis were overrepresented (P = 8.9E-9), as virtually every single gene in the chlorophyll biosynthetic pathway was repressed in response to TRV (Supplemental Fig. S1). The overrepresentation of genes encoding enzymes related to secondary metabolism, predominantly to the synthesis of isoprenoids, flavonoids, and phenylpropanoids, in the repressed gene set was highly significant in leaves (P = 5.3E-7). The stress category was clearly overrepresented among the induced genes (P = 1.4E-5), which mostly included genes related to abiotic stimuli (P = 9.8E-5; Fig. 2B). This subbin contained preferentially genes involved in cold, drought, and salt stresses. Photosynthesis and chlorophyll biosynthesis genes were not included in the stress category, so the bias detected in these two categories was not due to the same genes. Likewise, the redox regulation was significantly overrepresented in the set of genes up-regulated by TRV in leaves (P = 5.9E-5). Protein metabolism was also collectively affected by TRV infection in leaf tissue due to the repression of genes involved in protein synthesis, and more specifically those related to the synthesis of ribosomal proteins, which were highly overrepresented in the set of down-regulated genes (P = 7.2E-22; Fig. 2C). Furthermore, subbins related to protein degradation and ubiquitin-dependent protein degradation were significantly altered by TRV ($P < 0.005$; 80% of the TRV-responsive genes categorized in the ubiquitin pathway were up-regulated; Supplemental Table S1). Genes related to lipid metabolism were also distinctively altered in response to TRV (P = 7E-4). More specifically, genes related to fatty acid synthesis and elongation (P = 3E-5) or fatty acid desaturation (P = 4E-4) were significantly overrepresented among the repressed TRV-responsive genes (Fig. 2D). Finally, the cell wall and tricarboxylic acid categories were also overrepresented in the pool of genes down-regulated by TRV in leaves (P = 2.7E-5 and P = 0.002, respectively).

Verification of Microarray Data

To independently support the microarray results, we examined the response to TRV infection of a subset

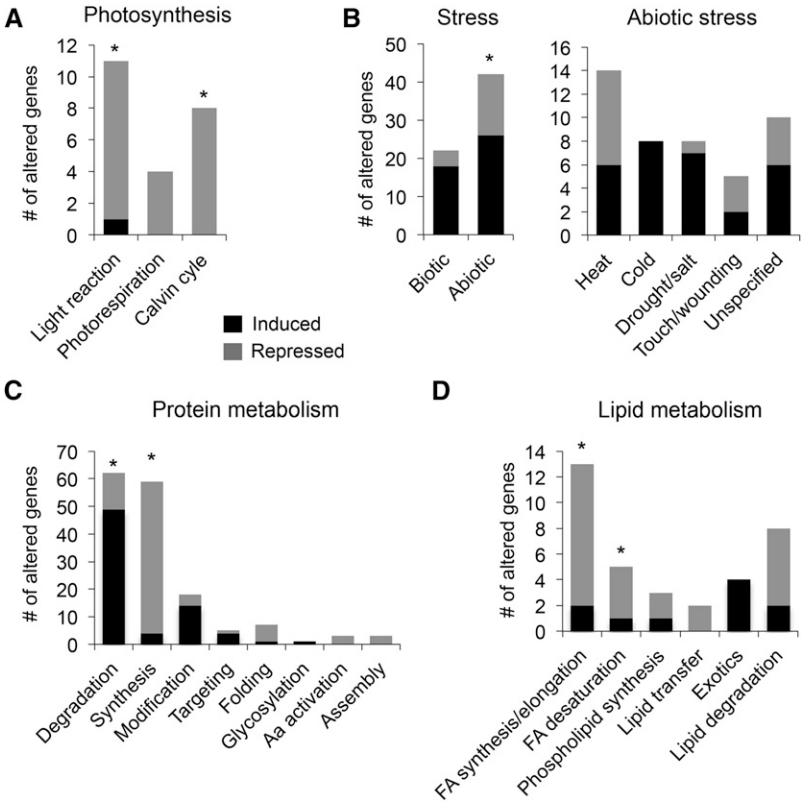

Figure 2. Distribution of TRV-responsive genes into enriched metabolic pathways and processes. Functional groups with significantly overrepresented genes are shown. A, Photosynthesis. B, Stress. C, Protein metabolism. D, Lipid metabolism. Classification of microarray data genes into subbins within each functional process (bin) was done using MapMan ontology. The number of induced (black bars) or repressed (gray bars) genes within each class is indicated. Statistically significant overrepresentation of altered genes within each subbin in each major functional category is indicated (Fisher's exact test, $*P < 0.001$). Aa, Amino acid; FA, fatty acid.

of genes representing both up- and down-regulation using qRT-PCR. To gain accuracy, the relative mRNA accumulation was measured on pooled RNA extracts obtained from independent sets of TRV-infected and mock-inoculated plants. These samples, therefore, were different from the ones used for microarray assays. The mRNA accumulation levels from genes related to photosynthesis (At3g55800 and At1g12900), protein synthesis (At2g32060 and At3g55280), chlorophyll biosynthesis (At3g51820 and At5g18660), protein degradation (At3g47160 and At4g10160), and stress responses (At2g29350 and At4g35770) were studied in leaf tissue (Fig. 3). Our results indicated that the expression of all these genes was significantly different (either induced or repressed) in the presence of TRV, consistent with microarray expression profiles (Supplemental Tables S1 and S2). Collectively, these data indicated that the alterations in gene expression detected by microarray analysis were good estimators of the transcriptional changes associated with virus infection.

Metabolic Responses to TRV Infection

To investigate the impact of TRV infection on primary metabolism, we determined global metabolic changes in systemically infected Arabidopsis leaves in a time-course experiment from 3 to 25 dpi. Metabolite profiling was performed using an established gas chromatography coupled to a time-of-flight mass spectrometry protocol (Lisec et al., 2006). In total, 47 metabolites were detected, and their levels were estimated relative to their concentration in mock-inoculated leaves collected at 3 dpi. The identified compounds were categorized as sugars and sugar alcohols (13), amino acids (22), organic acids (eight), and other metabolites (four; Supplemental Table S3). The data obtained by GC-MS for TVR-infected and mock-inoculated control leaves during the time-course assay (Supplemental Table S4) were examined by principal component analysis (PCA), with two principal components explaining 83.5% of the overall variance of the metabolite profiles (75.4% and 8% for principal component 1 [PC1] and principal component 2 [PC2], respectively; Fig. 4). The analysis highlights a clear metabolic shift among age of the leaves and developmental stage (from 3 to 25 dpi). To identify the underlying biological process, the principal component loadings were analyzed for overrepresentation and are described in Supplemental Table S5. As one might anticipate, the time course along infection was reflected as the main source of variance (Fig. 4). In addition, PC2 defined a clear separation of TRV-infected samples from their respective controls at each time point (except for 12 dpi) in the PCA score plot, which suggests that TRV infection produces significant metabolic changes during the infection (Fig. 4). We suspect that these metabolic differences could be more significant if we assume that the sampling strategy adopted in this study (collected tissue is presumably a mixture of infected and non-infected cells) likely results in the loss or dilution of

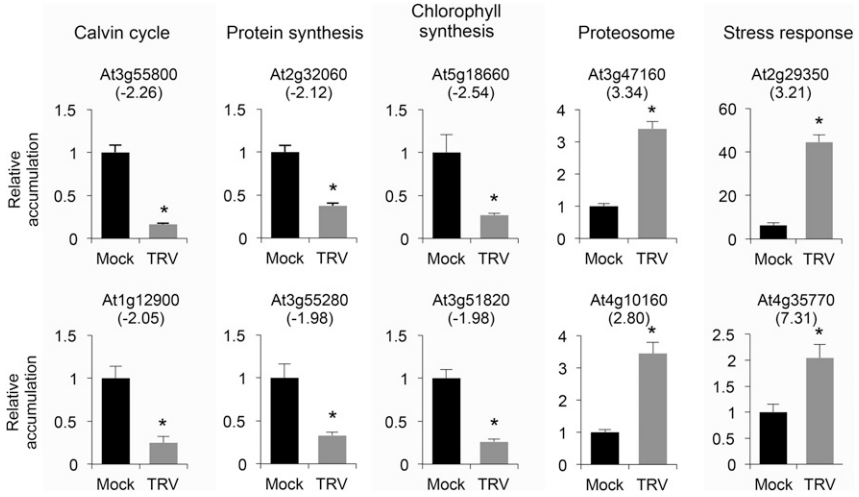

Figure 3. Confirmation of microarray data. Transcript accumulation of TRV-responsive genes from enriched functional categories was estimated by qRT-PCR at 8 dpi using an independent set of samples (not used for microarray analysis). Transcript levels in TRV-infected plants are given relative to those in mock-inoculated plants that were arbitrarily assigned a value of 1 after normalization to the *TUB5* internal control. Differences from mock-inoculated control values were significant at $P < 0.001$ (*; Duncan's multiple range test). The fold change for each gene calculated using microarray data is shown in parentheses. At3g55800, SEDOHEPTULOSE-BISPHOSPHATASE; At1g12900, GLYCERALDEHYDE 3-PHOSPHATE DEHYDROGENASE A SUBUNIT 2; At2g32060, RIBOSOMAL PROTEIN L7Ae/L30e/S12e/Gadd45 family protein; At3g55280, RIBOSOMAL PROTEIN L23A2; At5g18660, PALE-GREEN AND CHLOROPHYLL *B* REDUCED2; At3g51820, PIGMENT DEFECTIVE325; At3g47160, RING/U-box superfamily protein; At4g10160, RING/U-box superfamily protein; At1g29910, CHLOROPHYLL *A*/*B*-BINDING PROTEIN3; At4g35770, SENESCENCE1.

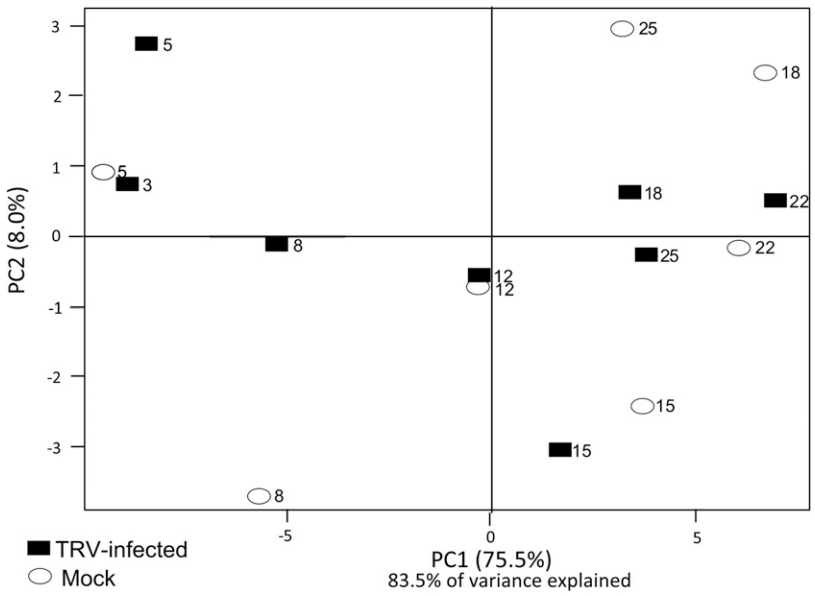

Figure 4. PCA of 47 identified metabolites by GC-MS. Leaf samples were collected at different time points from mock-inoculated (ovals) and TRV-infected (rectangles) Arabidopsis plants. The numbers indicate days after mock and TRV inoculation. The variance explained by each component (%) is given in parentheses.

quantitative information (Swarbrick et al., 2006; Yang et al., 2007).

TRV Infection and Sugar Metabolism

A total of 13 sugars were determined in samples from systemically infected rosette leaves. We used a PCA analysis to discriminate the effects of time and virus infection on the sugar component. In the PCA score plot of sugar compounds, time course was again the dominant source of variance underlying PC1, as demonstrated by a gradient from 3 to 25 dpi, where TRV infection is the main basis for PC2 separation (Supplemental Fig. S2A). Interestingly, this separation between infected and noninfected plants was particularly significant at 8 dpi, concurrent with the highest accumulation of TRV RNA (Fig. 1A).

Comparative measurements of their relative levels revealed an age-dependent increase in the content of most sugars identified, reaching a maximum at 18 to 22 dpi, except for trehalose, which gradually decreased, and Glc, Rha, Suc, and Xyl, which, in general, remained at comparable levels throughout the time course (Fig. 5A). Interestingly, we monitored a shift in the decrease from 18 to 22 dpi in the accumulation of Gal, galactinol, and raffinose in TRV-infected leaves (Fig. 5A). Moreover, in comparison with mock-inoculated leaves, only Fuc displayed higher content in TRV-infected leaves at later time points, while Fru, Glc, Man, and Gal showed a slight, albeit statistically significant, decrease at this time point in TRV-infected leaves ($P < 0.05$; Fig. 5A). In contrast, the relative levels of maltose, isomaltose, and trehalose were higher in noninfected leaves relative to TRV-infected leaves at the earlier time points tested ($P < 0.05$; Fig. 5A). Furthermore, these results obtained at 8 dpi were highly reproducible using an independent set of samples, indicating the robustness of our data (Supplemental Table S6).

We wondered if this carbohydrate boost was attributable to starch hydrolase activities, which might be expected to promote the conversion of starch into soluble sugars (Tecsi et al., 1994; Shalitin and Wolf, 2000; Love et al., 2005a; Smith et al., 2005). Therefore, we next measured starch levels in leaves from four independent replicates of mock- and TRV-inoculated plants. Our analysis showed that starch content was slightly, but not significantly, lower in TRV-infected leaves at 8 dpi (Fig. 5B). This result contrasted with microarray data that plastidial *β-AMYLASE4* (At5g55700) and *PHOSPHOGLUCAN WATER DIKINASE* (*PWD*; At5g26570) genes, both involved in starch degradation, were significantly enriched in the TRV-infected leaves at 8 dpi ($P < 0.01$; Supplemental Table S1), whereas *STARCH SYNTHASE2* (At3g01180) and *GRANULE-BOUND STARCH SYNTHASE1* (At1g32900), which is responsible for amylose synthesis, were both differentially repressed by TRV ($P < 0.01$; Supplemental Table S2). Time-course analysis of *PWD* mRNA using qRT-PCR corroborated the significant up-regulation of this gene in TRV-infected plants at 5, 8, and 18 dpi (Fig. 5C). To assess the effect of *PWD*-related activities on TRV multiplication, we inoculated a single knockout *pwd* mutant. Expression analysis of TRV RNA1 by qRT-PCR indicated reduced, but not significant, levels in *pwd*-infected plants (Fig. 5D), suggesting that inactivation of *PWD* alone was not sufficient to drastically alter TRV accumulation.

TRV Infection and Amino Acid and Organic Acid Metabolism

PCA was also used to identify changes in the amino acid and organic acid contents. The time parameter

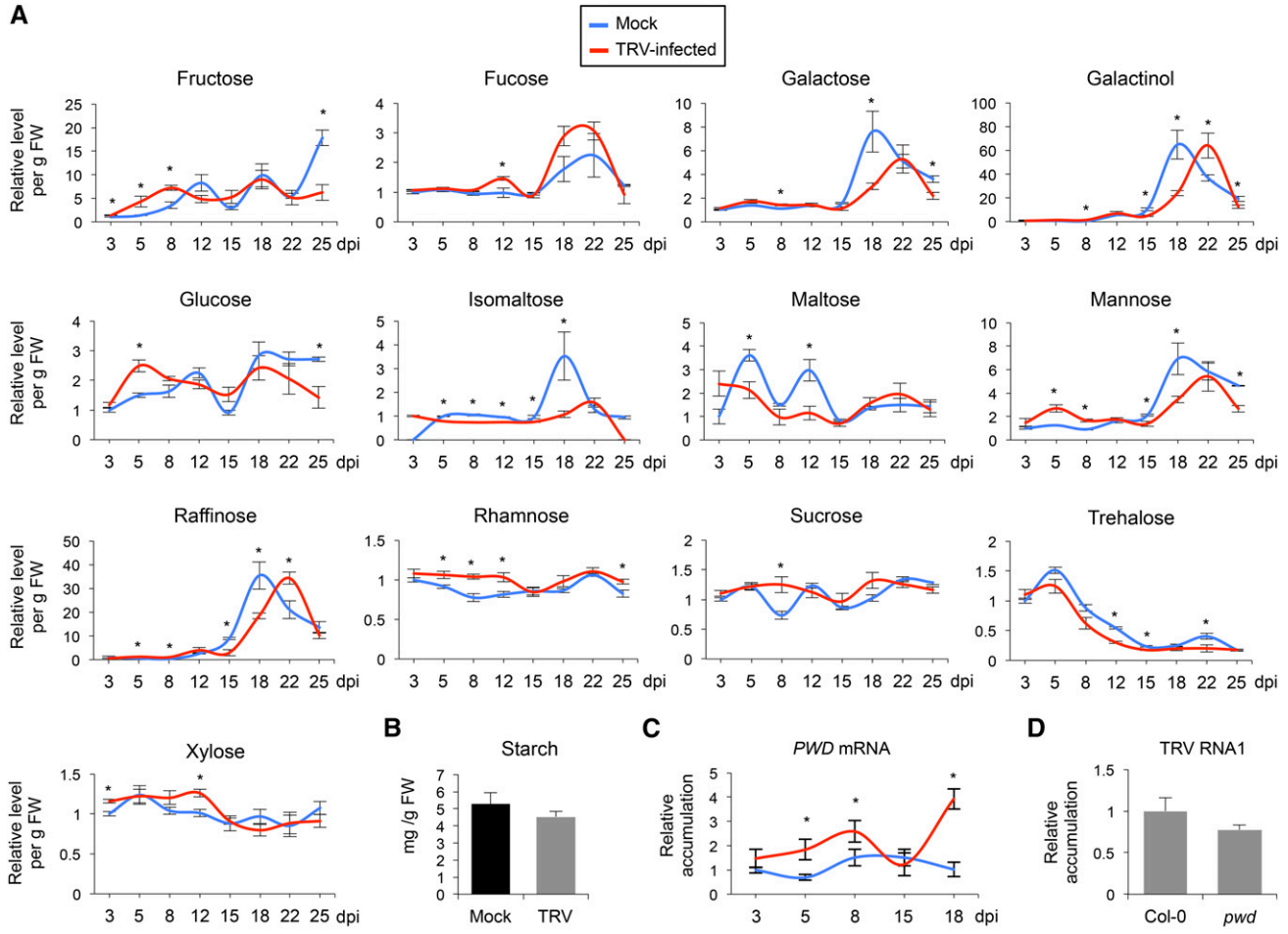

Figure 5. Effect of TRV infection on sugar levels in Arabidopsis. A, Sugar content was quantified in a time-course experiment by GC-MS on TRV-infected (red traces) and mock-inoculated (blue traces) leaves. Relative amounts were calculated with respect to the mock-inoculated controls at 3 dpi that were arbitrarily set at 1. Data are means ± SD from four independent biological replicates. Asterisks indicate statistical significance versus the mock-inoculated controls (Student's *t* test, $P < 0.05$). FW, Fresh weight. B, Starch content determined by enzymatic assay in TRV-infected (gray bar) and mock-inoculated (black bar) leaves at 8 dpi. C, Time-course accumulation of *PWD* transcripts in TRV-infected (red) and mock-inoculated (blue) Arabidopsis leaves determined by qRT-PCR. Values are related to the mock-inoculated sample at 3 dpi that was arbitrarily assigned to 1 after normalization to the *TUB5* internal control. Differences from mock-inoculated control values were significant at $P < 0.001$ (*; Duncan's multiple range test). D, Relative accumulation of TRV genomic RNA in *pwd* knockout mutants examined by qRT-PCR at 8 dpi. Values are given relative to those in wild-type plants, set at 1.

again reflected the main source of variance underlying PC1, whereas infection is the main basis for PC2 separation (Supplemental Fig. S2, B and C). The effect of TRV infection on the amino acid component was particularly striking when comparing PC1 and PC4 (Supplemental Fig. S2D). In general, we observed an increase in amino acid content, reaching a maximum peak at 8 and/or 12 dpi, following by steady decrease until 22 dpi (Fig. 6A; Supplemental Fig. S3). Nearly half of the amino acids identified exhibited TRV-responsive patterns that were particularly significant at 8 dpi, indicating that infection was an important modulator of the amino acid content in host cells. For instance, Ala, β-Ala, Gly, Ile, Phe, Pro, 4-hydroxy-Pro, Ser, Thr, Trp, and Val were significantly more abundant in the presence of TRV at 8 to 12 dpi (Fig. 6A; Supplemental Fig. S3). Similar results at 8 dpi were found when an independent set of samples was tested (Supplemental Table S6).

In order to shed light on the origin of changes in the amino acid profile in TRV-infected plants, we investigated perturbations in the expression of genes related to protein and amino acid metabolism. The transcriptomic data at 8 dpi revealed the repression of genes encoding ribosomal proteins, whereas genes encoding components of the ubiquitin-proteasome pathway displayed increased transcript accumulation in TRV-infected leaves (Fig. 2C; Supplemental Tables S1 and S2). This finding suggests that TRV could actively trigger selective protein breakdown events in

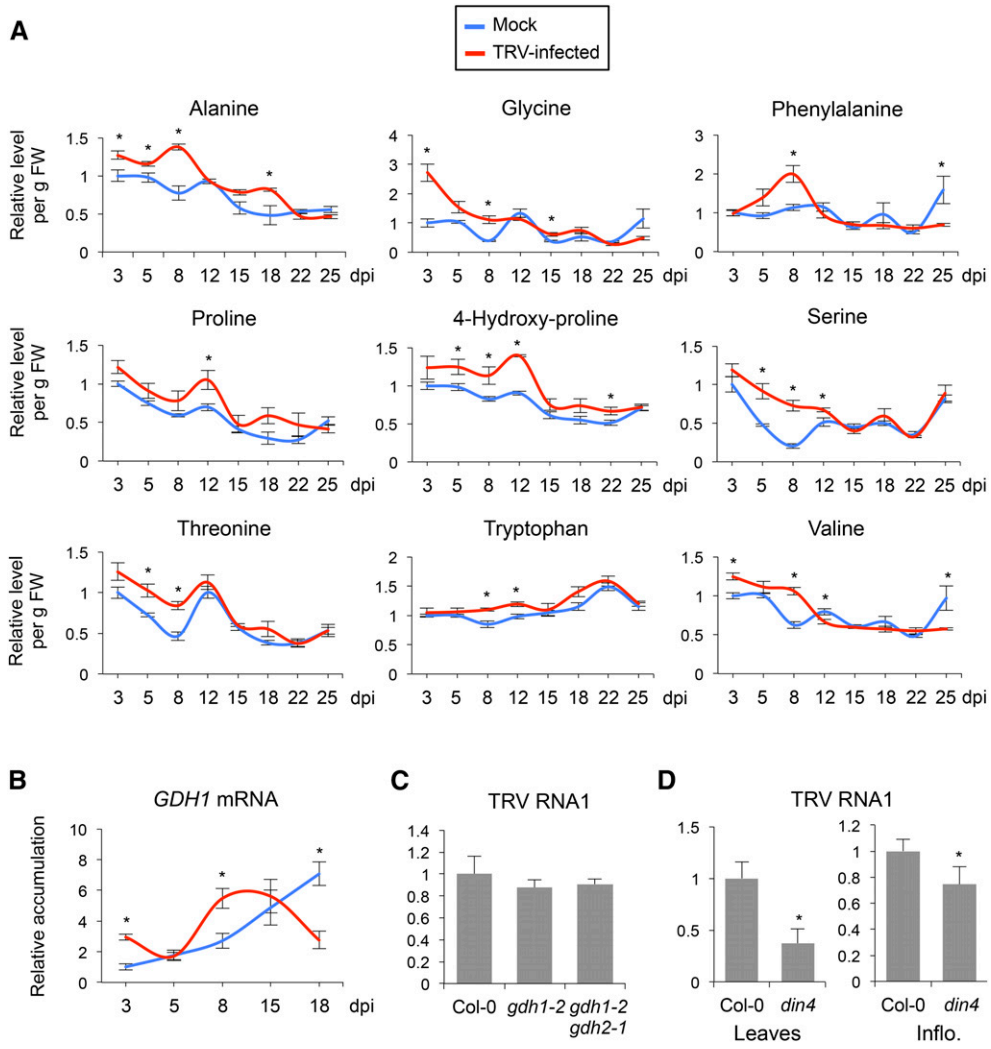

Figure 6. Effect of TRV infection on amino acid levels in Arabidopsis. Amino acid content was quantified in a time-course experiment by GC-MS on TRV-infected (red traces) and mock-inoculated (blue traces) leaves. Relative amounts were calculated with respect to the mock-inoculated controls at 3 dpi that were arbitrarily set at 1. Data are means ± SD from four independent biological replicates. Only amino acids that showed significant increases in TRV-infected leaves with respect to mock-inoculated samples are illustrated (Student's *t* test, $*P < 0.05$). FW, Fresh weight. B, Time-course accumulation of *GDH1* transcripts in leaves from TRV-infected plants (red trace) and mock-inoculated controls (blue trace). Values are related to the mock-inoculated sample at 3 dpi that was arbitrarily assigned to 1 after normalization to the *TUB5* internal control. C, Relative accumulation of TRV genomic RNA in leaves of the knockout mutants *gdh1-2* and *gdh1-2 gdh2-1* compared with wild-type backgrounds. D, Relative accumulation of TRV genomic RNA in leaves and inflorescences of the knockout mutant *din4* compared with wild-type controls. TRV RNA levels were estimated by qRT-PCR at 8 dpi (leaves) or 12 dpi (inflorescences), and levels detected in Col-0 wild-type plants were arbitrarily set at 1. Differences from mock-inoculated control values were significant at $P < 0.001$ (*; Duncan's multiple range test).

this tissue. Upon protein breakdown, the resultant amino acids can either enter the tricarboxylic acid cycle directly after conversion into the tricarboxylic acid intermediate 2-oxoglutarate or be catabolized to pyruvate or acetyl-CoA before entering the energy-generating tricarboxylic acid cycle (Araújo et al., 2011). Our microarray data provided partial evidence in support of both of these possible routes; thus, we wanted to explore their contribution to TRV infection. Microarray data supported by qRT-PCR indicated that the expression of *GLUTAMATE DEHYDROGENASE1* (*GDH1*; At5g18170) was strongly induced at 8 dpi in TRV-infected leaves compared with mock-inoculated plants (Fig. 6B; Supplemental Table S1). GDH1 converts Glu into 2-oxoglutarate and free ammonium, and its expression is tightly up-regulated under severe carbon shortage conditions (Forde and Lea, 2007). However, both Glu and most of the organic acids measured in mock-inoculated and TRV-infected leaves in a time-course experiment, including the tricarboxylic

acid cycle intermediates citrate, malate, fumarate, pyruvate, and succinate, had comparable levels in both cases tested (Supplemental Fig. S4A). This apparent discrepancy could be due to the rapid flux of metabolic intermediates and reactions through the tricarboxylic acid cycle. To test the contribution of *GDH1* to TRV susceptibility, we monitored TRV accumulation in *gdh1*- and *gdh2*-defective Arabidopsis mutants. qRT-PCR assays revealed that TRV accumulated to statistically similar levels in *gdh1-2* and *gdh1-2 gdh2-1* mutants compared with wild-type plants, indicating that GDH1 activity was not critical for virus infection (Fig. 6C).

Alterations in the levels of the branched-chain amino acids Val and Ile at 8 dpi (Fig. 6A; Supplemental Fig. S3) concurred with the differential expression of *DARK-INDUCIBLE4* (*DIN4*; At3g13450) and *BRANCHED-CHAIN AMINO ACID TRANSAMINASE2* (*BCAT2*; At1g10070) when comparing TRV-infected and mock-inoculated plants on the microarray (Supplemental Table S1). Both genes, *DIN4* and *BCAT2*, are involved in the sequential degradation of branched-chain amino acids to yield different acetyl-CoA derivatives (Binder, 2010). In order to better understand the effect of *DIN4* on TRV infection in Arabidopsis, we infected the loss-of-function *din4* Arabidopsis mutant. Interestingly, the TRV genomic RNA levels were significantly lower in both leaves and inflorescences of the mutant than in wild-type plants, which suggests that *DIN4* contributes to plant susceptibility (Fig. 6D). We did not observe appreciable differences in susceptibility to TRV using 35S-driven *DIN4* overexpressor transgenic lines (data not shown). In all cases, identical results were obtained in at least two independent replicates.

TRV Infection Interferes with Fatty Acid Biosynthesis

Other than acting as a tricarboxylic acid cycle precursor, acetyl-CoA molecules are the building blocks for fatty acid biosynthesis (Harwood, 2005). Therefore, we next turned our attention to address the question of whether TRV infection could alter the synthesis of lipids in Arabidopsis leaves. Our gene expression analysis revealed a significant repression of several critical genes involved in the biosynthesis of very-long-chain fatty acids (VLCFAs; C20–C34). For instance, the cytosolic *ACETYL-COENZYME A CARBOXYLASE1* gene (*ACC1*; At1g36160), which encodes the enzyme that catalyzes the carboxylation of acetyl-CoA to form malonyl-CoA in the cytosol, was down-regulated in the microarray (Baud et al., 2003; Supplemental Table S7). In addition, the *MALONYL-COENZYME A DECARBOXYLASE* gene (At4g04320), which is responsible for the reverse reaction, appeared induced in our analysis, suggesting that the initial step in VLCFA biosynthesis is tightly regulated during infection. Our gene expression data also indicated the repression of several genes downstream in the pathway, such as *LONG-CHAIN ACYL-COENZYME A SYNTHETASE2* (*LACS2*; At1g49430; Schnurr et al., 2004), or those that belong to the endoplasmic reticulum-bound acyl-CoA elongase enzymatic complex (Joubès et al., 2008). In particular, transcripts of the condensing enzyme 3-KETOACYL-COENZYME A SYNTHASE1 (KCS1; At1g01120), KCS3 (At1g07720), KCS8 (At2g15090), and KCS19 (At5g04530) were all decreased in expression in infected leaves compared with mock-inoculated leaves. Furthermore, several genes involved in plastidial fatty acid biosynthesis were repressed in infected leaves compared with the mock-inoculated ones (Supplemental Table S7). For example, this was the case for the β2-subunit of the plastidial pyruvate kinase (At1g32440), which catalyzes the irreversible synthesis of pyruvate used for acetyl-CoA synthesis (Andre et al., 2007), the *ACYL-CARRIER PROTEIN4* gene (*ACP4*; At4g25050), which encodes the most abundant ACP isoform in Arabidopsis leaves (Bonaventure and Ohlrogge, 2002), and *β-HYDROXYACYL-ACP DEHYDRATASE* (At2g22230), which is part of the fatty acid synthase complex (Brown et al., 2009).

To assess whether the down-regulation of genes involved in fatty acid biosynthesis was concurrent with reduced lipid content, we carried out the lipid analysis of Arabidopsis leaves at 3, 5, and 8 dpi. The total lipid content and fatty acid composition as well as the content and fatty acid composition of individual lipids did not show significant changes between TRV-infected and mock-inoculated plants at 3 and 5 dpi (Fig. 7A; Supplemental Table S8). However, we did observe major differences in the fatty acid composition of total lipids between infected and control samples at 8 dpi, although no significant changes in the total lipid content were detected (Fig. 7A; Table I). These changes in lipid and fatty acid metabolism at 8 dpi occurred concomitantly with elevated TRV levels in infected leaves (Fig. 1A). Particularly, the content of the trienoic fatty acids palmitolinolenic acid and linolenic acid was decreased in infected leaves (Fig. 7A). With respect to lipid classes, increases in the lipids of the Kennedy pathway, phosphatidic acid (PA), diacylglycerol (DAG), and triacylglycerol (TAG), were observed in leaves of TRV-infected plants at 8 dpi, whereas the content of chloroplastic galactolipids such as monogalactosyldiacylglycerol (MGDG) and digalactosyldiacylglycerol (DGDG), and phospholipids such as phosphatidylcholine, phosphatidylethanolamine, phosphatidylserine, and phosphatidylglycerol (PG), was reduced (Table I). Additionally, a reduction in the percentage of palmitic acid and an increase in those of linoleic and linolenic acids were detected in PA from infected leaves. In contrast, oleic and linoleic acids were increased and linolenic acid was decreased in chloroplast lipids such as MGDG, DGDG, and sulfonoquinovosyldiacylglycerol (SQ) of the same tissue (Table I). Interestingly, in another experiment corresponding to a different infection event, we found that the content of linoleic and linolenic acids was increased in the neutral lipids DAG and TAG in infected leaves (Supplemental Table S9). This enhancement coincided with the corresponding reduction in the percentage of the saturated fatty acids palmitic acid and

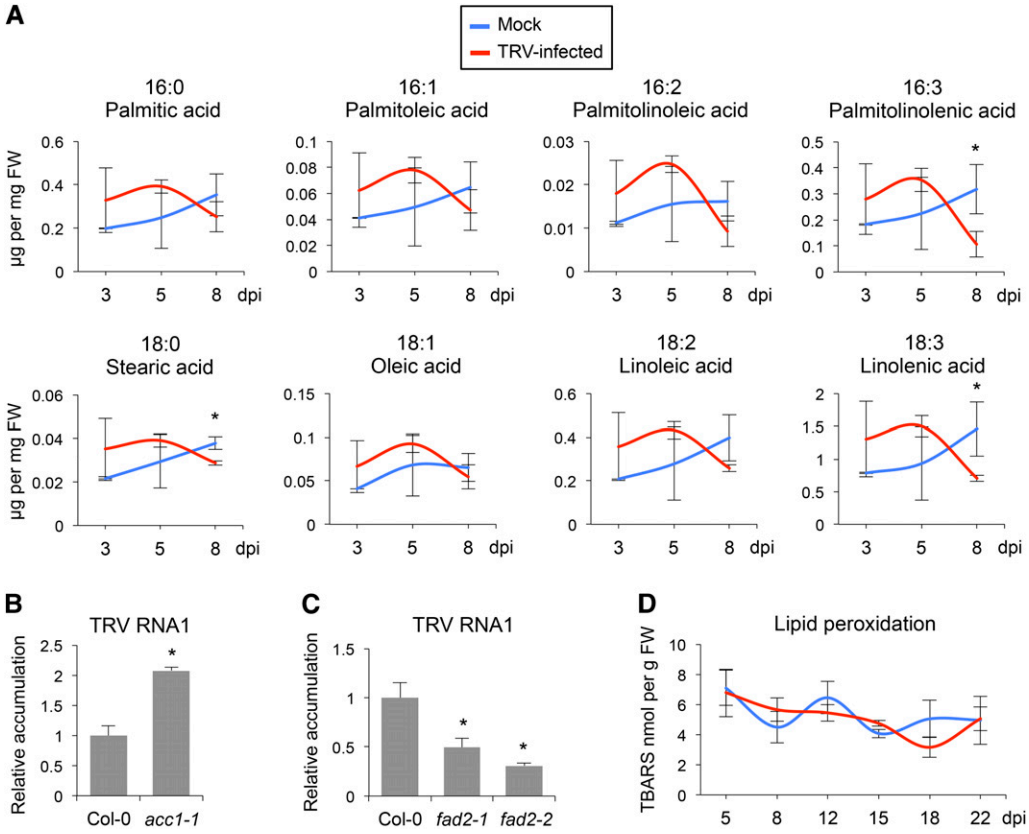

Figure 7. Effect of TRV infection on fatty acid composition in Arabidopsis. A, Fatty acid composition was analyzed in a time-course experiment by gas chromatography on TRV-infected (red traces) and mock-inoculated (blue traces) leaves. Data are means ± SD from three independent biological replicates. Asterisks indicate statistical significance versus the mock-inoculated controls (Student's *t* test, $P < 0.05$). B and C, Relative accumulation of TRV genomic RNA in *acc1-1* (B) and *fad2-1* and *fad2-2* (C) mutants examined by qRT-PCR at 8 dpi. Values are given relative to those in Col-0 plants, set at 1, after normalization to the *TUB5* internal control. Differences from mock-inoculated control values were significant at $P < 0.001$ (*; Duncan's multiple range test). D, Effect of TRV infection on lipid peroxidation (measured as thiobarbituric acid-reactive substances [TBARS]) at different time points after inoculation on TRV-infected (red trace) and mock-inoculated (blue trace) leaves. FW, Fresh weight.

stearic acid within the same lipid classes (Supplemental Table S9). These changes in fatty acid composition during TRV infection are consistent with our microarray data, which reveal an increase in the expression of the extraplastidial oleate desaturase gene (FATTY ACID DESATURASE2 [FAD2]; At3g12120), which catalyzes the desaturation of oleic acid to linoleic acid, and a repression of several chloroplast fatty acid desaturase genes (*FAD5* [At3g15850], *FAD6* [At4g30950], and *FAD8* [At5g05580]; Supplemental Table S7).

In order to determine if perturbations in the biosynthesis of VLCFA could modulate Arabidopsis susceptibility to TRV infection, we chose to investigate the effect of *ACC1* on virus infection by inoculating rosette leaves from Columbia-0 (Col-0) wild-type plants and transfer DNA insertion *acc1-1* mutants. The *acc1-1* mutation is recessive and embryo lethal in the homozygous state; thus, heterozygous plants were used in our analysis (Baud et al., 2003). Heterozygous plants appear normal except for the production of some severely wrinkled seeds that are unable to germinate (Baud et al., 2003). qRT-PCR reproducibly demonstrated that the TRV levels were substantially higher in plants with dysfunctional ACC1 ($P < 0.001$), suggesting that plant susceptibility to TRV can be manipulated during infection by interfering with VLCFA biosynthesis (Fig. 7B). Finally, to check if alterations in polyunsaturated fatty acid biosynthesis could affect Arabidopsis susceptibility to TRV infection, rosette leaves from Col-0 wild-type plants and two allelic *fad2-1* and *fad2-2* mutants were inoculated. The *fad2* mutants of Arabidopsis are deficient in the activity of endoplasmic reticulum oleate desaturase (FAD2); as a result, all the major phospholipids of the extrachloroplast membranes showed very reduced levels of polyunsaturated fatty acids (Miquel and Browse, 1992). As shown in Figure 7C, TRV levels determined by qRT-PCR were significantly lower in *fad2-1* and *fad2-2* compared with wild-type plants at 8 dpi, indicating that up-regulation of *FAD2* expression was related to a higher susceptibility of the plant to TRV infection. In addition to being required for

Table I. *Effect of TRV infection on the content and fatty acid composition of lipid classes in Arabidopsis leaves at 8 dpi*

Fatty acid composition was analyzed by gas chromatography. Data are means ± SD from three independent biological replicates. 16:0, Palmitic acid; 16:1, palmitoleic acid; 16:3, palmitolinolenic acid; 18:0, stearic acid; 18:1, oleic acid; 18:2, linoleic acid; 18:3, linolenic acid; ND, not detected; PC, phosphatidylcholine; PE, phosphatidylethanolamine; PI, phosphatidylinositol; PS, phosphatidylserine. Statistical differences from the mock treatment are indicated in boldface (Student's *t* test, $P < 0.05$).

Lipid Class	Treatment	Fatty Acid Composition							Total Content
		16:0	16:1	16:3	18:0	18:1	18:2	18:3	
					%				$\mu g\ mg^{-1}$ *fresh wt*
DAG	Mock	34.35 ± 4.32	ND	ND	36.54 ± 10.55	13.79 ± 2.49	12.12 ± 4.19	3.20 ± 4.53	0.005 ± 0.00
	TRV	28.88 ± 5.66	ND	ND	26.93 ± 1.35	**27.00 ± 2.08**	7.65 ± 0.27	9.54 ± 5.20	**0.007 ± 0.00**
TAG	Mock	27.27 ± 2.52	ND	ND	16.83 ± 2.06	30.33 ± 1.81	12.61 ± 0.50	12.97 ± 1.77	0.009 ± 0.00
	TRV	23.79 ± 3.81	ND	ND	19.14 ± 4.50	34.33 ± 7.97	10.36 ± 1.81	12.37 ± 6.85	**0.010 ± 0.00**
PA	Mock	31.74 ± 4.54	ND	ND	21.87 ± 0.52	7.62 ± 1.61	21.50 ± 1.80	17.26 ± 1.66	0.015 ± 0.00
	TRV	25.97 ± 4.14	ND	ND	**4.93 ± 0.22**	5.40 ± 0.35	**33.39 ± 1.72**	**30.30 ± 2.29**	**0.043 ± 0.00**
PC	Mock	27.14 ± 0.95	0.41 ± 0.05	ND	5.19 ± 0.70	8.19 ± 0.87	31.51 ± 0.46	27.57 ± 0.71	0.194 ± 0.00
	TRV	30.34 ± 3.59	0.54 ± 0.09	ND	3.77 ± 0.34	**6.60 ± 0.26**	29.84 ± 1.96	28.91 ± 1.78	**0.121 ± 0.01**
PE	Mock	33.37 ± 2.48	ND	ND	5.05 ± 0.30	3.19 ± 0.39	36.09 ± 1.26	22.29 ± 1.59	0.110 ± 0.01
	TRV	33.42 ± 1.31	ND	ND	**3.34 ± 0.41**	2.62 ± 0.01	37.26 ± 0.53	23.35 ± 0.36	**0.081 ± 0.00**
PI	Mock	45.84 ± 1.76	ND	ND	10.21 ± 0.85	4.03 ± 0.46	19.93 ± 0.45	19.99 ± 0.91	0.030 ± 0.00
	TRV	44.81 ± 7.14	ND	ND	9.04 ± 3.74	2.89 ± 0.31	21.65 ± 2.39	21.61 ± 1.32	0.025 ± 0.00
PS	Mock	26.54 ± 0.66	ND	ND	28.36 ± 2.11	7.35 ± 0.71	18.04 ± 2.50	19.72 ± 0.98	0.009 ± 0.00
	TRV	22.86 ± 4.46	ND	ND	23.44 ± 3.91	9.28 ± 2.02	23.43 ± 0.23	20.98 ± 1.23	**0.006 ± 0.00**
PG	Mock	31.81 ± 1.20	22.84 ± 0.86	ND	3.63 ± 0.27	6.27 ± 0.41	7.00 ± 0.38	28.45 ± 1.52	0.115 ± 0.01
	TRV	33.70 ± 1.02	24.16 ± 0.72	ND	2.80 ± 0.00	**7.60 ± 0.39**	7.85 ± 0.22	**23.90 ± 0.13**	**0.081 ± 0.01**
MGDG	Mock	2.73 ± 2.29	0.89 ± 0.07	27.23 ± 4.10	1.25 ± 0.38	1.16 ± 0.04	2.21 ± 0.34	64.52 ± 2.01	0.444 ± 0.09
	TRV	2.64 ± 0.36	**1.99 ± 0.37**	27.82 ± 0.31	1.72 ± 0.49	**1.96 ± 0.21**	**3.06 ± 0.30**	**60.81 ± 0.68**	**0.174 ± 0.02**
DGDG	Mock	16.07 ± 0.39	0.23 ± 0.04	2.04 ± 0.05	3.43 ± 0.11	1.31 ± 0.06	3.62 ± 0.08	73.29 ± 0.68	0.152 ± 0.02
	TRV	**20.56 ± 0.66**	ND	2.02 ± 0.02	2.81 ± 0.18	**1.70 ± 0.02**	**4.66 ± 0.02**	**68.26 ± 1.55**	0.101 ± 0.01
SQ	Mock	8.73 ± 0.15	ND	ND	15.53 ± 1.79	4.76 ± 0.70	20.47 ± 2.12	50.50 ± 0.76	0.018 ± 0.00
	TRV	7.84 ± 0.78	ND	ND	9.24 ± 0.60	**7.57 ± 0.44**	33.68 ± 0.57	**41.67 ± 2.14**	0.012 ± 0.00

low-salt and low-temperature tolerance in Arabidopsis, the involvement of the *FAD2* gene in response to biotic stress has been widely documented (Miquel et al., 1993; Kirsch et al., 1997; Wang et al., 2004; Zhang et al., 2012). In this scenario, accumulation of polyunsaturated fatty acids could compensate for losses caused by the elimination of lipid hydroperoxides during the oxidative burst (Kirsch et al., 1997). However, although the production of reactive oxygen species (ROS) has been reported in cells infected with plant viruses (Díaz-Vivancos et al., 2008), the levels of lipid peroxidation were not significantly altered in response to TRV compared with control plants (Fig. 7D).

TRV Infection and Abiotic Stress Tolerance

Our microarray data indicated extensive overlapping in the transcriptional responses triggered by TRV and those broadly reported in stressed plants (Fig. 2B; Fujita et al., 2006). Besides, several metabolite compounds, such as sugar derivatives, amino acids, amines, and conjugated polyunsaturated fatty acids, detected at elevated levels in TRV-infected leaves have known roles in plant tolerance to various environmental stresses (Yancey et al., 1982; Browse et al., 1986; Xu et al., 2008). This finding prompted us to investigate if TRV-responsive metabolites could enhance plant tolerance to stress during TRV infection. Among them, we chose to test the role of putrescine in plant tolerance, because putrescine levels increased over 2-fold in response to TRV infection at 5 and 8 dpi in our assay (Fig. 8A). Furthermore, elevated putrescine levels were consistent with the significant induction of the stress-induced putrescine biosynthetic genes *ARGININE DECARBOXILASE1* (*ADC1*; At2g16500) and *ADC2* (At4g34710) in response to TRV accumulation, as measured by qRT-PCR in a time-course experiment (these two genes were not represented in the CATMA; Fig. 8B). Given that the accumulation of putrescine is essential for Arabidopsis cold acclimation and survival at freezing temperatures (Kasukabe et al., 2004; Cuevas et al., 2008), we wanted to investigate if plants systemically infected with TRV exhibited higher tolerance to cold stress. To test this idea, plants at 21°C were sequentially placed in a low-temperature growth chamber at 4°C for 1 h and then at −6°C for 6 h. The effect of freezing was estimated by counting the number of survival plants producing inflorescences and siliques. Our results indicated that approximately 67% of plants infected with TRV (n = 267) survived and produced siliques, whereas approximately 48% of mock-inoculated plants (n = 287) were tolerant to frost treatment (Fig. 8C). This result indicated that plants infected with TRV were more tolerant to freezing than noninfected plants. Both putrescine overaccumulation and higher tolerance to freezing in TRV-infected plants were reproducibly observed in an independent experiment (Supplemental Fig. S5). Then, to evaluate the physiological role of putrescine in freezing tolerance associated with TRV infection, we conducted a similar experiment using the Arabidopsis *adc1-2* mutant, which is defective in putrescine biosynthesis and displays a moderate reduction in freezing tolerance (Cuevas et al., 2008). In our experimental conditions, we found that approximately 45% and 55% of mock-inoculated (n = 180) and TRV-infected (n = 225) plants survived, respectively. Thus, the loss of function of *ADC1* led to reduced freezing tolerance, which was particularly clear in TRV-infected plants (Fig. 8C). These results indicated that putrescine was at least partially responsible for the phenotype of increased tolerance associated with TRV infection in Arabidopsis. Finally, we investigated the effect of *ADC1* and *ADC2* genes on TRV infection by using two *adc1* and *adc2* mutant alleles. qRT-PCR demonstrated that TRV RNA was significantly more abundant in TRV-infected mutants than in the Col-0 background at 8 dpi, suggesting that putrescine has a protective role against virus infection in Arabidopsis (Fig. 8D).

DISCUSSION

In this study, we profiled mRNA transcript abundance and metabolite content in Arabidopsis leaves infected systemically with TRV. The virus elicited general responses that are generic to different viruses in susceptible hosts alongside responses that were apparently specific to TRV (Whitham et al., 2003; Yang et al., 2007; Rodrigo et al., 2012). Changes in host gene expression and primary metabolism were prominent in infected leaves, where diverse functional categories of genes could be significantly recognized as TRV responsive. An intriguing question is how all these responses contribute to the many aspects (from basic compatibility to basal defense) of the infective process in plants. In this work, gene expression data supported by metabolomics studies were used to investigate how primary metabolism is altered upon TRV infection and how alterations in primary metabolism contribute to modulate plant susceptibility to TRV infection.

Our data indicated that TRV infection promotes the accumulation of several soluble sugars at the time points of maximal TRV titers in infected leaves. We found that transient accumulation of sugars did not stimulate the conversion of soluble sugars into starch in infected leaves, since starch levels were comparable (with only a trend to diminish) in mock-inoculated and TRV-infected leaves. Such negative regulation of starch synthesis might be related to the repression of photosynthesis and chlorophyll biosynthesis genes that we detected during the infection. As reported previously, photosynthetic repression is likely related to a negative feedback regulation due to elevated hexose levels in infected leaves (Bolton, 2009). Perturbations in the photosynthetic apparatus are known to result in stomatal closure, so it is possible that TRV infection could impair stomatal opening as documented in many other plant-virus pathosystems

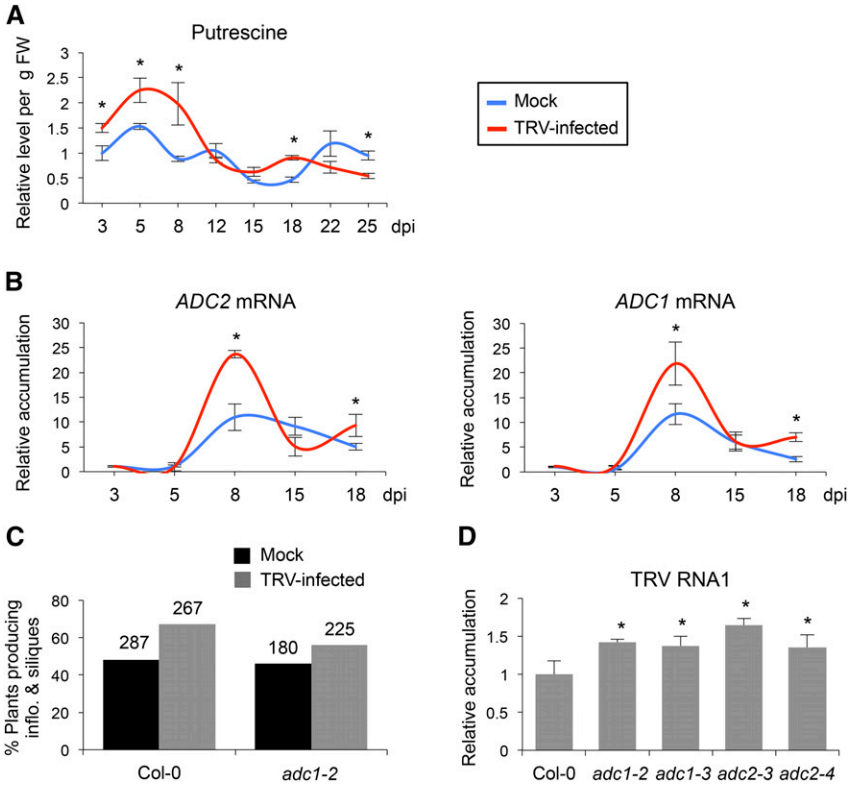

Figure 8. Effect of putrescine on TRV infection and improved tolerance to freezing during infection. A, Putrescine levels were quantified in a time-course experiment by GC-MS on TRV-infected (red trace) and mock-inoculated (blue trace) leaves. Relative amounts were calculated with respect to the mock-inoculated control at 3 dpi that was arbitrarily set at 1. Data are means ± SD from four independent biological replicates. Asterisks indicate statistical significance versus the mock-inoculated controls (Student's *t* test, $P < 0.05$). FW, Fresh weight. B, Time-course accumulation of *ADC1* and *ADC2* transcripts in TRV-infected (red traces) and mock-inoculated (blue traces) Arabidopsis leaves determined by qRT-PCR. Values are related to the mock-inoculated sample at 3 dpi that was arbitrarily assigned to 1 after normalization to the *TUB5* internal control. Differences from mock-inoculated control values were significant at $P < 0.001$ (*; Duncan's multiple range test). C, Percentage of mock-inoculated (black bars) and TRV-infected (gray bars) Arabidopsis plants showing enhanced tolerance to freezing in the Col-0 and *adc1-2* genetic backgrounds. The total number of tested plants is indicated above each bar. Tolerance was estimated as the percentage of plants producing inflorescences and siliques. D, Relative accumulation of TRV genomic RNA in several *adc1* and *adc2* knockout mutants examined by qRT-PCR at 8 dpi. Values are given relative to those in wild-type plants, set at 1. *$P < 0.001$ (Duncan's multiple range test).

(Grimmer et al., 2012). If so, the restriction of CO_2 supply caused by stomatal closure would lead to a reduction in the capacity for starch synthesis.

As documented previously, we showed that Suc was abundant in leaves infected with TRV at 8 dpi. In those other studies, elevations in Suc concentration were linked to higher starch hydrolase activities and low starch contents in infected plants (Tecsi et al., 1994; Shalitin and Wolf, 2000). In our assay, the up-regulation of *PWD*, which is involved in starch breakdown, did not lead to reduced starch content. However, the lower levels of trehalose in TRV-infected leaves could be diagnostic of starch degradation, as a decrease in trehalose accelerates starch degradation under high demands of Suc (Lunn et al., 2014). Also, we detected increased accumulation of Xyl, Fuc, and Man at 12 dpi in TRV-infected leaves. These sugars are components of both structural and storage carbohydrate polymers and act as recycling products derived from the turnover of polysaccharides and other sugar-containing metabolites. Nevertheless, the effect of TRV on starch hydrolysis to produce Suc remains to be tested. Whether the export of Suc to sink organs was impaired also remains to be investigated. Our data indicated that TRV infection promoted the expression of several genes with carbohydrate transmembrane transporter activity, in agreement with the sugar accumulation response triggered by TRV in Arabidopsis leaves. TRV-induced monosaccharide carriers such as the *TONOPLAST MONOSACCHARIDE TRANSPORTER1* (At1g20840), the Gal-specific *SUGAR TRANSPORT PROTEIN14* (*STP14*; At1g77210), or the hexose-specific *STP13* (At5g26340) plasma membrane transporters could all help to increase selective monosaccharide import into stressed leaves. We did not find evidence of the induction of plant invertases in infected

tissues that could accelerate the release of hexoses from Suc in response to the pathogen (Roitsch and González, 2004). Nevertheless, the increase in hexose sugars (Glc and Fru) suggests a reprogramming in the carbohydrate flux at early time points of infection.

Most of the sugars that exhibited TRV responsiveness are known to accumulate to a high extent in multiple plant-pathogen interactions. In addition to their roles as carbon and energy sources, they might function as signaling molecules in plant defense and the maintenance of cellular homeostasis (Berger et al., 2007; Bolouri Moghaddam and Van den Ende, 2012). For instance, Suc and Rha are known to stimulate the accumulation of protective agents such as flavonoids (i.e. anthocyanins) and other secondary metabolites (Watt et al., 2004; Treutter, 2005; Bolouri Moghaddam and Van den Ende, 2012). However, the significant repression of genes related to the biosynthesis of flavonoids and phenylpropanoids in TRV-infected leaves partly argues against this possibility (Supplemental Table S2). Our analysis revealed a significant contribution of raffinose, Gal, and galactinol to the TRV-associated metabolome. Strikingly, these three compounds presented similar profiles over time, being moderately, but significantly, more abundant at 8 dpi in TRV-infected plants than in control plants. They also exhibited a significant delay in their peaks of abundance in TRV-infected plants relative to the control ones. Raffinose is synthesized from Suc by the subsequent addition of activated Gal donated by galactinol (Peterbauer et al., 2001). Since galactinol and raffinose could act as scavengers of ROS (Nishizawa et al., 2008), we speculate that they may alleviate the stressful conditions imposed by the enhanced production of ROS during the infection. Generation of ROS has been documented in plants undergoing both compatible and incompatible viral infections (Love et al., 2005b), and in our assay, we monitored a significant induction of several genes associated with the detoxification of ROS, such as catalases, superoxide dismutase, glutathione peroxidase, and ascorbate peroxidase (Supplemental Table S1). This finding suggests that ROS are generated in response to TRV. Furthermore, galactinol and probably also raffinose are involved as signals to trigger plant immunity under pathogen attack (Kim et al., 2008).

Our transcriptomic data pointed to a significant repression of genes encoding ribosomal proteins as well as increased transcripts encoding components of the ubiquitin-proteasome pathway. This finding is in agreement with that observed for other Arabidopsis-infecting viruses, such as *Cabbage leaf curl virus*, *Cucumber mosaic virus*, and *Turnip mosaic virus* (Marathe et al., 2004; Yang et al., 2007; Hwang et al., 2011). It is not clear, however, whether elevated amino acid levels in infected leaves are due to selective protein breakdown in this tissue or higher rates of biosynthesis. It would also be of interest to test how transcriptomic changes in protein metabolism are reflected in the rate of protein synthesis of the cell. In our study, the accumulation of Ser and Gly to high levels at early time points of infection may be related to the transcriptional repression of photorespiration that we observed (Timm et al., 2013). Indeed, higher accumulation of the photorespiratory intermediates Ser and Gly is known to cause a feedback deregulation of photorespiration-related genes (Timm et al., 2013). The accumulation of several other amino acids could reveal antiviral responses in infected leaves. High concentrations of the osmoprotectant Pro and 4-hydroxy-Pro in response to TRV may contribute to enhanced stress tolerance in infected cells, as observed previously in bromo mosaic virus-infected rice (*Oryza sativa*) plants (Kishor et al., 1995; Xu et al., 2008). It is also worth mentioning that TRV did not elicit significant changes in the accumulation of the γ-aminobutyrate (GABA) shunt, which involves GABA, Glu, and Gln (Fait et al., 2008). GABA rapidly accumulates in response to biotic stress, and it has been postulated that it has important functions related to defense (Fait et al., 2008). Other TRV-responsive amino acids have the potential to be used a precursors in the biosynthesis of defense signal molecules. For instance, the accumulation of Val could fuel the synthesis of aliphatic glucosinolates in Arabidopsis, where they play a key role in innate immune responses (Sønderby et al., 2010). Phe is also the precursor of benzenic glucosinolates and a major starting compound in the phenylpropanoid biosynthetic pathway, but down-regulation of genes in this pathway raises questions about its potential role in defense via the conversion to phenylpropanoids. Elevated Trp may potentiate the biosynthesis of a large variety of secondary metabolites like terpenoid indole alkaloids, indolic glucosinolates, and indolic phytoalexins (Facchini, 2001; Sønderby et al., 2010). A relevant question is whether the increments in amino acid levels reflect the biosynthesis of antimicrobial compounds. Also, the elucidation of how these amino acids contribute to plant defense against plant viruses will certainly require additional scientific effort.

The elevation of Ala concentration in TRV-infected leaves was consistent with the induction of *ALANINE-2-OXOGLUTARATE AMINOTRANSFERASE2* (*AOAT2*; At1g70580) and *ALANINE-GLYOXYLATE AMINOTRANSFERASE3* (*AGT3*; At2g38400). Given that AOAT2 and AGT3 are involved in both the synthesis and degradation of Ala, and that Ala concentration increases in infected leaves, it is unclear whether TRV induces these two genes to stimulate Ala biosynthesis from pyruvate or, in contrast, Ala degradation into pyruvate. Previous studies demonstrated that Ala aminotransferases are crucial for the conversion of Ala to pyruvate during plant recovery from low-oxygen stresses, when Ala is produced in relatively large amounts (Sousa and Sodek, 2003; Miyashita et al., 2007). We observed a significant increase of pyruvate levels at 5 dpi and, to a lower extent, 8 dpi, suggesting that TRV may favor the catabolic direction. We showed that TRV infection interferes with branched-chain amino acid metabolism by up-regulating the expression of

DIN4 and *BCAT2*. More importantly, *DIN4* induction was beneficial for the virus, since the genetic inactivation of this gene drastically compromised TRV proliferation in infected plants. It is unclear, however, how TRV benefits from high *DIN4* transcript levels. The likely consequence of the induction of *DIN4* in infected plants is the production of acetyl-CoA derivatives via branched-chain amino acid catabolism (Binder, 2010). Since acetyl-CoA can readily enter the tricarboxylic acid cycle, it is tempting to speculate that TRV stimulates this pathway to power the synthesis of ATP (Araújo et al., 2010). Likewise, high levels of Thr may eventually feed the tricarboxylic acid cycle. However, we did not find significant differences in the relative accumulation of tricarboxylic acid intermediates between TRV-infected and mock-inoculated plants, and our microarray data revealed a significant repression of genes within this functional category in response to TRV. Induction of *GDH1* might also be seen as a means to stimulate protein respiration as an alternative energy source during infection. However, the contribution of *GDH1* to the infection process may be trivial given the negligible effect of single and double *gdh* mutations on TRV accumulation.

We found that TRV-mediated interference with VLCFAs and plastidial fatty acid biosynthesis was critical for virus infection. We reasoned that the repression of *ACC1* during TRV infection represents a major advantage to the virus, since *acc1* mutants contained higher levels of TRV. Given that VLCFAs are used in cuticular wax formation (Pollard et al., 2008), down-regulation of *ACC1* as well as *LACS2* and several isoforms of *KCS* could negatively affect normal cuticle development, producing a phenotype of enhanced susceptibility to TRV. Interestingly, gene expression data were not fully consistent with the analysis of lipids, since TRV infection did not cause major changes in the total lipid content. This is not entirely surprising, however, since plastidial fatty acid biosynthesis is a primary metabolic pathway and a complete block of the route would not be anticipated (Harwood, 2005). TRV predominantly interacted with the VLCFA branch of the pathway, and VLCFAs represent a very minor percentage in the fatty acid composition of total lipids (Joubès et al., 2008). On the other hand, the observed increase of linoleic acid and the decrease of linolenic acid detected in chloroplast lipids such as MGDG, DGDG, SQ, and PG are consistent with the detected induction of the extraplastidial oleate desaturase *FAD2* and the repression of the plastidial desaturases *FAD5*, *FAD6*, and *FAD8* in infected leaves. The involvement of the *FAD2* gene in the response to biotic stresses has been described in parsley (*Petroselinum crispum*) cell cultures supplemented with a fungal elicitor (Kirsch et al., 1997) and in fungus-infected avocado (*Persea americana*) fruits (Wang et al., 2004). In these cases, it has been suggested that the accumulation of polyunsaturated fatty acids could compensate for losses caused by the elimination of lipid hydroperoxides from membrane injury during the oxidative burst and/or by the conversion of polyunsaturated fatty acids to signal molecules such as jasmonates (Kirsch et al., 1997). As opposed to findings in other susceptible plant-virus interactions, lipid peroxidation was not significant in TRV-infected leaves (Díaz-Vivancos et al., 2008; García-Marcos et al., 2009). Since TRV levels were significantly lower in Arabidopsis *fad2* mutants than in wild-type plants, induction of *FAD2* could favor virus infection by redirecting oleic acid desaturation into linoleic acid instead of being elongated to VLCFAs, which are utilized in cuticular wax formation. In this manner, up-regulation of *FAD2* could negatively affect normal cuticle development, as in the case of down-regulation of *ACC1*.

We found that approximately 60% of the genes stimulated by TRV infection were also induced during dark-induced senescence (Lin and Wu, 2004). Similarly, TRV-infected plants accumulated a vast array of metabolites with known function as osmoprotectants involved in stress tolerance. For instance, galactinol and raffinose, which were abundant in the presence of TRV, are known to contribute to improving the tolerance of oxidative damage caused by chilling stress (Nishizawa et al., 2008). This illustrates the idea that, to cope with some extreme conditions, plants use a common set of regulatory and metabolic pathways that entails similar reprogramming of gene expression and metabolite accumulation (Bohnert et al., 1995). As a result, plants benefit from this vast array of infection-associated responses by increasing their tolerance to stress. In our study, we observed metabolic acclimation in TRV-infected plants by means of the accumulation of protective metabolites. More specifically, we demonstrated that putrescine accumulation during infection makes the plants more acclimated to freezing stress. By using *adc1* and *adc2* mutants, in which the biosynthesis of putrescine is compromised, we demonstrated that putrescine accumulation is necessary to an enhanced development of chilling tolerance in Arabidopsis upon infection. It would be worth testing the stress-protective effect associated with the accumulation of other TRV-responding metabolites. Furthermore, our data suggest that putrescine may act as a signaling molecule to transduce defense responses, given that both the *adc1* and *adc2* mutants were hypersusceptible to TRV infection. In this line, the polyamine spermine is also thought to function as a signal that enhances photorespiration in the defense response of Arabidopsis to cucumber mosaic virus infection (Mitsuya et al., 2009).

MATERIALS AND METHODS

Plant Material and TRV Inoculation

Arabidopsis (*Arabidopsis thaliana*) plants were grown in controlled-environment chambers under 16 h of light at 19°C to 22°C. Arabidopsis mutant homozygous lines for *pwd* (isolated from the original line SALK_110814), *din4-1* (SALK_088551C), *gdh1-1* (European Arabidopsis Stock Centre identifier

N3975; donated by Gloria M. Coruzzi and Rosana Melo-Olivera, New York University), *gdh1-2 gdh2-1* (generated by crossing homozygous mutants from the original lines SALK_042736 and SALK_102711), and the heterozygous *acc1-1* (SALK_087627) were obtained from the European Arabidopsis Stock Centre. All homozygous mutant SALK lines used in this study were PCR genotyped. The homozygous *fad2-1* and *fad2-2* mutant alleles were kindly provided by John Browse (Institute of Biological Chemistry, Washington State University). The homozygous *adc1* and *adc2* mutant seeds were donated by Teresa Altabella (Centre for Research in Agricultural Genomics, University of Barcelona). All mutants were in the ecotype Col-0 background.

Arabidopsis plants were sap inoculated on rosette leaves at 20 d after germination using inoculum prepared from *Nicotiana benthamiana* leaves systemically infected after agroinfiltration of the infectious clone TRV-*N. benthamiana* PHYTOENE DESATURASE or TRV-GFP as described (Donaire et al., 2008). Arabidopsis control plants were mock inoculated with extracts from healthy leaves and processed as the infected plants. RNA-blot hybridization using a TRV-specific radiolabeled DNA probe and/or reverse transcription (RT)-PCR using TRV-specific primers were used to confirm that every single TRV-inoculated plant was infected and that each mock-inoculated plant was free of virus. Primer sequences are listed in Supplemental Table S10.

Microarray and Statistical Analysis

Total RNA was extracted with the Plant RNeasy kit (Qiagen) from Arabidopsis young rosette leaves at growth stage 3.6 (Boyes et al., 2001). To reduce biological errors due to natural variation, poly(A) mRNA from three independent biological replicates was processed using the CATMA, which contains 24,576 gene-specific tags corresponding to 21,690 unigenes (version 2.2; Crowe et al., 2003; Hilson et al., 2004). Each replicate consisted of RNA pooled from at least 20 plants. Positive infection for every single inoculated plant was confirmed by RT-PCR using TRV-specific primers, while samples from mock-inoculated plants were confirmed as virus free (data not shown). RNA integrity was checked with the Experion Automated Electrophoresis System (Bio-Rad). The microarray analysis was carried out at the Unité de Recherche en Génomique Végétale. One technical replication with fluorochrome reversal was performed for each biological replicate (i.e. six hybridizations). The RT of RNA in the presence of Cy3 deoxy-UTP or Cy5 deoxy-UTP (PerkinElmer; http://las.perkinelmer.com), the hybridization of labeled samples to the slides, and the scanning of the slides were performed as described (Lurin et al., 2004).

Experiments were designed with the statistics group of the Unité de Recherche en Génomique Végétale. The statistical analysis was based on three dye swaps (i.e. six arrays each containing 24,576 gene-specific tags and 384 controls) as described (Lurin et al., 2004). The controls were used for assessing the quality of the hybridizations but were not included in the statistical tests or the graphical representation of the results. For each array, the raw data comprised the logarithm of median feature pixel intensity at wavelengths 635 nm (red) and 532 nm (green). No background was subtracted. Log_2 ratio refers to the differential expression between two conditions. It is either $\log_2$ (red/green) or $\log_2$ (green/red) according to the experimental design. Array-by-array normalization was performed to remove systematic biases. To determine differentially expressed genes, a paired Student's t test on the $\log_2$ ratios was done, assuming that the variance of the $\log_2$ ratios was the same for all genes. Spots displaying extreme variances were excluded. The raw P values were adjusted by the Bonferroni method, which controls the family-wise error rate. We considered genes with a Bonferroni P value lower than 1% as being differentially expressed. The fold change is calculated by the following formula: fold change = 2^ (signal $\log_2$ I mock/TRV; if signal $\log_2$ ratio ≥ 0) or fold change = $(-1) \times 2^{\wedge}$ ($-1 \times$ signal $\log_2$ ratio; if signal $\log_2$ ratio < 0). The microarray data are available at GSE15557.

Functional Annotation of TRV-Responsive Genes and Overrepresentation Analysis

The list of Arabidopsis genes with statistically altered expression due to TRV infection was imported into the MapMan software (Thimm et al., 2004), which allows microarray data to be assigned to any known plant metabolic pathways or processes (bins). A Wilcoxon rank-sum test implemented in MapMan was used to extract functional groups (bins) whose members exhibited a significantly different regulation compared with all other remaining bins in the data set (Benjamani and Hochberg-corrected $P < 0.05$). Fisher's exact test then was used to test for significant overrepresentation of the number of genes within the MapMan bins.

qRT-PCR Assay

qRT-PCR was performed in a Rotor-Gene 6000/Rotor-Gene Q real-time PCR machine (Corbett/Qiagen) using the thermal protocol as follows: 48°C for 30 min; 95°C for 10 min; and 40 cycles of 95°C for 30 s, 64°C for 30 s, and 72°C for 20 s. RT-PCR was carried out in a final volume of 15 μL containing 7.5 μL of Biotools QuantiMix EASY SYG, 2.55 μL of RNase-free water, 0.075 μL of Moloney murine leukemia virus reverse transcriptase, 0.075 μL of RNase inhibitor, 0.9 μL of each primer at 5 μM, and 3 μL of total RNA extract (RNA at 10 ng μL^{-1}). A no-template control was also included in each run for each gene. *β-TUBULIN5* (*TUB5*; At1g20010) was chosen for normalization because of its similar level of expression in mock-inoculated and TRV-infected tissues. Each experiment was conducted in three technical replicates with at least two samples for each treatment. Relative viral accumulation and gene expression were determined for each reaction using the Delta-delta cycle threshold method and Rotor-Gene 6000 Series Software (Corbett). All qRT-PCR assays were done using independent RNA samples not used for microarray hybridizations. Primer sequences are listed in Supplemental Table S10.

Determination of Metabolite Levels by GC-MS

Leaf samples from four independent biological replicates were collected according to a time-course scheme, each replicate consisting of a pool of at least 15 plants. Young rosette leaves from TRV-infected plants and the corresponding mock-inoculated plants were harvested at the same leaf position in order to minimize the effect of variation in the metabolite content throughout the plant. Furthermore, the infection of every single plant used in this assay was confirmed previously, and mock-inoculated controls were shown to be free of virus. Collected tissue was immediately frozen in liquid nitrogen and stored at −80°C until further analysis. Extraction was performed by grinding of tissue in liquid nitrogen and immediate addition of the appropriate extraction buffer. Derivatization and gas chromatography coupled to time-of-flight mass spectrometry analyses were carried out as described (Lisec et al., 2006). Metabolites were identified by comparison to database entries of authentic standards, and relative quantification was performed as described (Lisec et al., 2006). The metabolite profiling data generated was then subjected to statistical analysis by Student's t test. Full documentation of metabolite profiling data acquisition and interpretation is provided in Supplemental Table S3 following recommended guidelines (Fernie et al., 2011).

Starch Analysis

Arabidopsis leaves were harvested at the end of the light period and frozen in liquid N_2. Approximately 0.5 g of frozen material was homogenized with a mortar and pestle and suspended in 45 mL of 50 mM HEPES, pH 7.6, and 1% (v/v) Triton X-100. The homogenate was filtered through one layer of 100-μm nylon mesh and centrifuged for 15 min at 4°C and 4,000g. The pellet was resuspended in 2 mL of 90% (v/v) Percoll and centrifuged for 40 min at 4°C and 10,000g. The starch pellet was washed six times with 96% (v/v) ethanol and finally air dried. The pellet was resuspended in 1 mL of 0.2 N KOH, boiled for 30 min, and centrifuged for 10 min at 14,000g at 4°C. Finally, the supernatant was adjusted to pH 5.5 with 1 N acetic acid and used to determine the starch amount as described (Lin et al., 1988). Four measurements were done per biological replicate.

Lipid Analysis

Arabidopsis leaf samples from three independent biological replicates were collected as indicated above. Total lipids were extracted with chloroform: methanol (1:2, v/v) as described (Bligh and Dyer, 1959), and lipid separation was carried out by thin-layer chromatography as described (Hernández et al., 2008). Fatty acid methyl esters of the individual lipid classes were produced by acid-catalyzed transmethylation (Garcés and Mancha, 1993) and analyzed by gas chromatography using a 7890A device (Agilent Technologies) fitted with a capillary column (30-m length, 0.25-mm i.d., 0.20-μm film thickness) of fused silica (Supelco) and a flame ionization detector. Hydrogen was used as the carrier gas with a linear flux of 1.34 mL min^{-1} and a split ratio of 1:50. The injector and detector temperature was 220°C, and the oven temperature was 170°C.

Lipid Peroxidation Assay

Lipid peroxidation was estimated by determining the concentration of TBARS, as described previously (García-Marcos et al., 2009). The absorbance of the samples was read at 532 nm. The value for nonspecific absorption at 600 nm was subtracted. The amount of TBARS was calculated from the extinction coefficient 155 mM^{-1} cm^{-1}. Four independent replicates from TRV-infected and mock-inoculated plants were analyzed.

Low-Temperature Treatments

Freezing assays were carried out in a temperature-programmable chamber. Plants at 12 dpi were moved to darkness at 4°C for 1 h. Then, temperature was lowered in 1°C increments per hour for 5.5 h to a maximum freezing temperature of −6°C, which was maintained for 6 h. The temperature then was raised again to 4°C at the same incremental rate. After thawing at 4°C for 1 h in the dark, plants were returned to their initial growth conditions. Tolerance to freezing was determined as the capacity of plants to produce new inflorescences and siliques.

Sequence data from this article can be found in the GenBank/EMBL data libraries under accession number GSE15557.

Supplemental Data

The following materials are available in the online version of this article.

Supplemental Figure S1. MapMan illustration of microarray data showing changes in the expression of genes involved in the tetrapyrrole biosynthetic pathway.

Supplemental Figure S2. PCA using metabolic profiling data from sugars, organic acids, and amino acids detected by GC-MS.

Supplemental Figure S3. Time-course accumulation of amino acids in mock-inoculated and TRV-infected Arabidopsis.

Supplemental Figure S4. Time-course accumulation of organic acids in mock-inoculated and TRV-infected Arabidopsis.

Supplemental Figure S5. Polyamine levels and tolerance to freezing.

Supplemental Table S1. Induced genes in TRV-infected Arabidopsis rosette leaves at 8 dpi.

Supplemental Table S2. Repressed genes in TRV-infected Arabidopsis rosette leaves at 8 dpi.

Supplemental Table S3. Overview of the metabolite reporting list.

Supplemental Table S4. Time-course profiling of primary metabolites in TRV-infected Arabidopsis.

Supplemental Table S5.- Overrepresentation analysis of the PCA loadings of metabolite data.

Supplemental Table S6. Metabolite profiling of TRV-infected Arabidopsis at 8 dpi (experiment 2).

Supplemental Table S7. Functional classification of TRV-responsive genes related to lipid metabolism in infected leaves.

Supplemental Table S8. Effect of TRV infection on the content and fatty acid composition of lipid classes in Arabidopsis leaves at 3 and 5 dpi.

Supplemental Table S9. Effect of TRV infection on the content and fatty acid composition of lipid classes in Arabidopsis leaves at 8 dpi (experiment 2).

Supplemental Table S10. List of primers used for qRT-PCR.

ACKNOWLEDGMENTS

We thank Llucia Martínez-Priego (Centro de Investigaciones Biológicas, Consejo Superior de Investigaciones Científicas) for technical assistance, Carlos Perea and Julio Salinas (Centro de Investigaciones Biológicas, Consejo Superior de Investigaciones Científicas) for excellent support in freezing experiments, and John Browse (Washington State University) and Teresa Altabella (Centre for Research in Agricultural Genomics) for sharing Arabidopsis mutant seeds.

Received September 12, 2014; accepted October 30, 2014; published October 30, 2014.

LITERATURE CITED

Almon E, Horowitz M, Wang HL, Lucas WJ, Zamski E, Wolf S (1997) Phloem-specific expression of the tobacco mosaic virus movement protein alters carbon metabolism and partitioning in transgenic potato plants. Plant Physiol **115:** 1599–1607

Andre C, Froehlich JE, Moll MR, Benning C (2007) A heteromeric plastidic pyruvate kinase complex involved in seed oil biosynthesis in *Arabidopsis*. Plant Cell **19:** 2006–2022

Araújo WL, Ishizaki K, Nunes-Nesi A, Larson TR, Tohge T, Krahnert I, Witt S, Obata T, Schauer N, Graham IA, et al (2010) Identification of the 2-hydroxyglutarate and isovaleryl-CoA dehydrogenases as alternative electron donors linking lysine catabolism to the electron transport chain of *Arabidopsis* mitochondria. Plant Cell **22:** 1549–1563

Araújo WL, Tohge T, Ishizaki K, Leaver CJ, Fernie AR (2011) Protein degradation: an alternative respiratory substrate for stressed plants. Trends Plant Sci **16:** 489–498

Balachandran S, Hull RJ, Martins RA, Vaadia Y, Lucas WJ (1997) Influence of environmental stress on biomass partitioning in transgenic tobacco plants expressing the movement protein of tobacco mosaic virus. Plant Physiol **114:** 475–481

Baud S, Guyon V, Kronenberger J, Wuillème S, Miquel M, Caboche M, Lepiniec L, Rochat C (2003) Multifunctional acetyl-CoA carboxylase 1 is essential for very long chain fatty acid elongation and embryo development in Arabidopsis. Plant J **33:** 75–86

Bazzini AA, Manacorda CA, Tohge T, Conti G, Rodriguez MC, Nunes-Nesi A, Villanueva S, Fernie AR, Carrari F, Asurmendi S (2011) Metabolic and miRNA profiling of TMV infected plants reveals biphasic temporal changes. PLoS ONE **6:** e28466

Berger S, Sinha AK, Roitsch T (2007) Plant physiology meets phytopathology: plant primary metabolism and plant-pathogen interactions. J Exp Bot **58:** 4019–4026

Binder S (2010) Branched-chain amino acid metabolism in Arabidopsis thaliana. The Arabidopsis Book **8:** e0137, doi/10.1199/tab.0137

Bligh EG, Dyer WJ (1959) A rapid method of total lipid extraction and purification. Can J Biochem Physiol **37:** 911–917

Bohnert HJ, Nelson DE, Jensen RG (1995) Adaptations to environmental stresses. Plant Cell **7:** 1099–1111

Bolouri Moghaddam MR, Van den Ende W (2012) Sugars and plant innate immunity. J Exp Bot **63:** 3989–3998

Bolton MD (2009) Primary metabolism and plant defense: fuel for the fire. Mol Plant Microbe Interact **22:** 487–497

Bonaventure G, Ohlrogge JB (2002) Differential regulation of mRNA levels of acyl carrier protein isoforms in Arabidopsis. Plant Physiol **128:** 223–235

Boyes DC, Zayed AM, Ascenzi R, McCaskill AJ, Hoffman NE, Davis KR, Görlach J (2001) Growth stage-based phenotypic analysis of *Arabidopsis*: a model for high throughput functional genomics in plants. Plant Cell **13:** 1499–1510

Brown A, Affleck V, Kroon J, Slabas A (2009) Proof of function of a putative 3-hydroxyacyl-acyl carrier protein dehydratase from higher plants by mass spectrometry of product formation. FEBS Lett **583:** 363–368

Browse J, McCourt P, Somerville C (1986) A mutant of Arabidopsis deficient in $C_{18:3}$ and $C_{16:3}$ leaf lipids. Plant Physiol **81:** 859–864

Choi YH, Kim HK, Linthorst HJ, Hollander JG, Lefeber AW, Erkelens C, Nuzillard JM, Verpoorte R (2006) NMR metabolomics to revisit the tobacco mosaic virus infection in Nicotiana tabacum leaves. J Nat Prod **69:** 742–748

Crowe ML, Serizet C, Thareau V, Aubourg S, Rouzé P, Hilson P, Beynon J, Weisbeek P, van Hummelen P, Reymond P, et al (2003) CATMA: a complete Arabidopsis GST database. Nucleic Acids Res **31:** 156–158

Cuevas JC, López-Cobollo R, Alcázar R, Zarza X, Koncz C, Altabella T, Salinas J, Tiburcio AF, Ferrando A (2008) Putrescine is involved in Arabidopsis freezing tolerance and cold acclimation by regulating abscisic acid levels in response to low temperature. Plant Physiol **148:** 1094–1105

Díaz-Vivancos P, Clemente-Moreno MJ, Rubio M, Olmos E, García JA, Martínez-Gómez P, Hernández JA (2008) Alteration in the chloroplastic metabolism leads to ROS accumulation in pea plants in response to plum pox virus. J Exp Bot **59:** 2147–2160

Donaire L, Barajas D, Martínez-García B, Martínez-Priego L, Pagán I, Llave C (2008) Structural and genetic requirements for the biogenesis of tobacco rattle virus-derived small interfering RNAs. J Virol **82:** 5167–5177

Espinoza C, Medina C, Somerville S, Arce-Johnson P (2007) Senescence-associated genes induced during compatible viral interactions with grapevine and Arabidopsis. J Exp Bot **58:** 3197–3212

Facchini PJ (2001) Alkaloid biosynthesis in plants: biochemistry, cell biology, molecular regulation, and metabolic engineering applications. Annu Rev Plant Physiol Plant Mol Biol **52:** 29–66

Fait A, Fromm H, Walter D, Galili G, Fernie AR (2008) Highway or byway: the metabolic role of the GABA shunt in plants. Trends Plant Sci **13:** 14–19

Fernie AR, Aharoni A, Willmitzer L, Stitt M, Tohge T, Kopka J, Carroll AJ, Saito K, Fraser PD, DeLuca V (2011) Recommendations for reporting metabolite data. Plant Cell **23:** 2477–2482

Forde BG, Lea PJ (2007) Glutamate in plants: metabolism, regulation, and signalling. J Exp Bot **58:** 2339–2358

Fujita M, Fujita Y, Noutoshi Y, Takahashi F, Narusaka Y, Yamaguchi-Shinozaki K, Shinozaki K (2006) Crosstalk between abiotic and biotic stress responses: a current view from the points of convergence in the stress signaling networks. Curr Opin Plant Biol **9:** 436–442

Garcés R, Mancha M (1993) One-step lipid extraction and fatty acid methyl esters preparation from fresh plant tissues. Anal Biochem **211:** 139–143

García-Marcos A, Pacheco R, Martiáñez J, González-Jara P, Díaz-Ruíz JR, Tenllado F (2009) Transcriptional changes and oxidative stress associated with the synergistic interaction between Potato virus X and Potato virus Y and their relationship with symptom expression. Mol Plant Microbe Interact **22:** 1431–1444

Grimmer MK, John Foulkes M, Paveley ND (2012) Foliar pathogenesis and plant water relations: a review. J Exp Bot **63:** 4321–4331

Harwood JL (2005) Fatty Acid Biosynthesis. Blackwell Publishing, Oxford

Herbers K, Meuwly P, Frommer WB, Metraux JP, Sonnewald U (1996) Systemic acquired resistance mediated by the ectopic expression of invertase: possible hexose sensing in the secretory pathway. Plant Cell **8:** 793–803

Herbers K, Takahata Y, Melzer M, Mock HP, Hajirezaei M, Sonnewald U (2000) Regulation of carbohydrate partitioning during the interaction of potato virus Y with tobacco. Mol Plant Pathol **1:** 51–59

Hernández ML, Guschina IA, Martínez-Rivas JM, Mancha M, Harwood JL (2008) The utilization and desaturation of oleate and linoleate during glycerolipid biosynthesis in olive (Olea europaea L.) callus cultures. J Exp Bot **59:** 2425–2435

Hilson P, Allemeersch J, Altmann T, Aubourg S, Avon A, Beynon J, Bhalerao RP, Bitton F, Caboche M, Cannoot B, et al (2004) Versatile gene-specific sequence tags for Arabidopsis functional genomics: transcript profiling and reverse genetics applications. Genome Res **14:** 2176–2189

Hwang IS, An SH, Hwang BK (2011) Pepper asparagine synthetase 1 (CaAS1) is required for plant nitrogen assimilation and defense responses to microbial pathogens. Plant J **67:** 749–762

Joubès J, Raffaele S, Bourdenx B, Garcia C, Laroche-Traineau J, Moreau P, Domergue F, Lessire R (2008) The VLCFA elongase gene family in Arabidopsis thaliana: phylogenetic analysis, 3D modelling and expression profiling. Plant Mol Biol **67:** 547–566

Kasukabe Y, He L, Nada K, Misawa S, Ihara I, Tachibana S (2004) Overexpression of spermidine synthase enhances tolerance to multiple environmental stresses and up-regulates the expression of various stress-regulated genes in transgenic Arabidopsis thaliana. Plant Cell Physiol **45:** 712–722

Kim HK, Choi YH, Verpoorte R (2010) NMR-based metabolomic analysis of plants. Nat Protoc **5:** 536–549

Kim MS, Cho SM, Kang EY, Im YJ, Hwangbo H, Kim YC, Ryu CM, Yang KY, Chung GC, Cho BH (2008) Galactinol is a signaling component of the induced systemic resistance caused by Pseudomonas chlororaphis O6 root colonization. Mol Plant Microbe Interact **21:** 1643–1653

Kirsch C, Hahlbrock K, Somssich IE (1997) Rapid and transient induction of a parsley microsomal Δ12 fatty acid desaturase mRNA by fungal elicitor. Plant Physiol **115:** 283–289

Kishor P, Hong Z, Miao GH, Hu C, Verma D (1995) Overexpression of Δ^1-pyrroline-5-carboxylate synthetase increases proline production and confers osmotolerance in transgenic plants. Plant Physiol **108:** 1387–1394

Lin JF, Wu SH (2004) Molecular events in senescing Arabidopsis leaves. Plant J **39:** 612–628

Lin TP, Caspar T, Somerville C, Preiss J (1988) Isolation and characterization of a starchless mutant of *Arabidopsis thaliana* (L.) Heynh lacking ADPglucose pyrophosphorylase activity. Plant Physiol **86:** 1131–1135

Lisec J, Schauer N, Kopka J, Willmitzer L, Fernie AR (2006) Gas chromatography mass spectrometry-based metabolite profiling in plants. Nat Protoc **1:** 387–396

López-Gresa MP, Lisón P, Kim HK, Choi YH, Verpoorte R, Rodrigo I, Conejero V, Bellés JM (2012) Metabolic fingerprinting of Tomato mosaic virus infected Solanum lycopersicum. J Plant Physiol **169:** 1586–1596

Love AJ, Martin T, Graham IA, Milner JJ (2005a) Carbohydrate partioning and sugar signalling in Cauliflower mosaic virus-infected turnip and Arabidopsis. Physiol Mol Plant Pathol **67:** 83–91

Love AJ, Yun BW, Laval V, Loake GJ, Milner JJ (2005b) Cauliflower mosaic virus, a compatible pathogen of Arabidopsis, engages three distinct defense-signaling pathways and activates rapid systemic generation of reactive oxygen species. Plant Physiol **139:** 935–948

Lunn JE, Delorge I, Figueroa CM, Van Dijck P, Stitt M (2014) Trehalose metabolism in plants. Plant J **79:** 544–567

Lurin C, Andrés C, Aubourg S, Bellaoui M, Bitton F, Bruyère C, Caboche M, Debast C, Gualberto J, Hoffmann B, et al (2004) Genome-wide analysis of *Arabidopsis* pentatricopeptide repeat proteins reveals their essential role in organelle biogenesis. Plant Cell **16:** 2089–2103

Marathe R, Guan Z, Anandalakshmi R, Zhao H, Dinesh-Kumar SP (2004) Study of Arabidopsis thaliana resistome in response to cucumber mosaic virus infection using whole genome microarray. Plant Mol Biol **55:** 501–520

Miquel M, Browse J (1992) Arabidopsis mutants deficient in polyunsaturated fatty acid synthesis: biochemical and genetic characterization of a plant oleoyl-phosphatidylcholine desaturase. J Biol Chem **267:** 1502–1509

Miquel M, James D Jr, Dooner H, Browse J (1993) Arabidopsis requires polyunsaturated lipids for low-temperature survival. Proc Natl Acad Sci USA **90:** 6208–6212

Mitsuya Y, Takahashi Y, Berberich T, Miyazaki A, Matsumura H, Takahashi H, Terauchi R, Kusano T (2009) Spermine signaling plays a significant role in the defense response of Arabidopsis thaliana to cucumber mosaic virus. J Plant Physiol **166:** 626–643

Miyashita Y, Dolferus R, Ismond KP, Good AG (2007) Alanine aminotransferase catalyses the breakdown of alanine after hypoxia in Arabidopsis thaliana. Plant J **49:** 1108–1121

Nishizawa A, Yabuta Y, Shigeoka S (2008) Galactinol and raffinose constitute a novel function to protect plants from oxidative damage. Plant Physiol **147:** 1251–1263

Peterbauer T, Lahuta LB, Blöchl A, Mucha J, Jones DA, Hedley CL, Gòrecki RJ, Richter A (2001) Analysis of the raffinose family oligosaccharide pathway in pea seeds with contrasting carbohydrate composition. Plant Physiol **127:** 1764–1772

Pollard M, Beisson F, Li Y, Ohlrogge JB (2008) Building lipid barriers: biosynthesis of cutin and suberin. Trends Plant Sci **13:** 236–246

Rodrigo G, Carrera J, Ruiz-Ferrer V, del Toro FJ, Llave C, Voinnet O, Elena SF (2012) A meta-analysis reveals the commonalities and differences in Arabidopsis thaliana response to different viral pathogens. PLoS ONE **7:** e40526

Roitsch T, González MC (2004) Function and regulation of plant invertases: sweet sensations. Trends Plant Sci **9:** 606–613

Schnurr J, Shockey J, Browse J (2004) The acyl-CoA synthetase encoded by LACS2 is essential for normal cuticle development in *Arabidopsis*. Plant Cell **16:** 629–642

Shalitin D, Wolf S (2000) Cucumber mosaic virus infection affects sugar transport in melon plants. Plant Physiol **123:** 597–604

Smith AM, Zeeman SC, Smith SM (2005) Starch degradation. Annu Rev Plant Biol **56:** 73–98

Sønderby IE, Geu-Flores F, Halkier BA (2010) Biosynthesis of glucosinolates: gene discovery and beyond. Trends Plant Sci **15:** 283–290

Sousa CAF, Sodek L (2003) Alanine metabolism and alanine aminotransferase activity in soybean (Glycine max) during hypoxia of the root system and subsequent return to normoxia. Environ Exp Bot **50:** 1–8

Swarbrick PJ, Schulze-Lefert P, Scholes JD (2006) Metabolic consequences of susceptibility and resistance (race-specific and broad-spectrum) in barley leaves challenged with powdery mildew. Plant Cell Environ **29:** 1061–1076

Tecsi LI, Maule AJ, Smith AM, Leegood RC (1994) Metabolic alterations in cotyledons of Cucurbita pepo infected with Cucumber mosaic virus. J Exp Bot **45:** 1541–1551

Thimm O, Bläsing O, Gibon Y, Nagel A, Meyer S, Krüger P, Selbig J, Müller LA, Rhee SY, Stitt M (2004) MAPMAN: a user-driven tool to display genomics data sets onto diagrams of metabolic pathways and other biological processes. Plant J **37:** 914–939

Timm S, Florian A, Wittmiß M, Jahnke K, Hagemann M, Fernie AR, Bauwe H (2013) Serine acts as a metabolic signal for the transcriptional control of photorespiration-related genes in Arabidopsis. Plant Physiol **162:** 379–389

Treutter D (2005) Significance of flavonoids in plant resistance and enhancement of their biosynthesis. Plant Biol (Stuttg) **7:** 581–591

Wang X, Beno-Moualem D, Kobiler I, Leikin-Frenkel A, Lichter A, Prusky D (2004) Expression of Delta(12) fatty acid desaturase during the induced accumulation of the antifungal diene in avocado fruits. Mol Plant Pathol **5:** 575–585

Watt G, Leoff C, Harper AD, Bar-Peled M (2004) A bifunctional 3,5-epimerase/4-keto reductase for nucleotide-rhamnose synthesis in Arabidopsis. Plant Physiol **134:** 1337–1346

Whitham SA, Quan S, Chang HS, Cooper B, Estes B, Zhu T, Wang X, Hou YM (2003) Diverse RNA viruses elicit the expression of common sets of genes in susceptible Arabidopsis thaliana plants. Plant J **33:** 271–283

Whitham SA, Yang C, Goodin MM (2006) Global impact: elucidating plant responses to viral infection. Mol Plant Microbe Interact **19:** 1207–1215

Wise RP, Moscou MJ, Bogdanove AJ, Whitham SA (2007) Transcript profiling in host-pathogen interactions. Annu Rev Phytopathol **45:** 329–369

Xu P, Chen F, Mannas JP, Feldman T, Sumner LW, Roossinck MJ (2008) Virus infection improves drought tolerance. New Phytol **180:** 911–921

Yancey PH, Clark ME, Hand SC, Bowlus RD, Somero GN (1982) Living with water stress: evolution of osmolyte systems. Science **217:** 1214–1222

Yang C, Guo R, Jie F, Nettleton D, Peng J, Carr T, Yeakley JM, Fan JB, Whitham SA (2007) Spatial analysis of Arabidopsis thaliana gene expression in response to Turnip mosaic virus infection. Mol Plant Microbe Interact **20:** 358–370

Zhang J, Liu H, Sun J, Li B, Zhu Q, Chen S, Zhang H (2012) Arabidopsis fatty acid desaturase FAD2 is required for salt tolerance during seed germination and early seedling growth. PLoS ONE **7:** e30355